

Enclosure 2

Metallic Materials Qualification for the Kairos Power Testing Program, Revision 1

(Non-Proprietary)



Kairos Power LLC
707 W. Tower Ave
Alameda, CA 94501

Metallic Materials Qualification for the Kairos Power Fluoride Salt-Cooled High-Temperature Reactor

Topical Report

Revision No. 1
Document Date: June 2021

Non-Proprietary

COPYRIGHT Notice

This document is the property of Kairos Power LLC (Kairos Power) and was prepared in support of the development of the Kairos Power Fluoride Salt-Cooled High Temperature Reactor (KP-FHR) design. Other than by the Nuclear Regulatory Commission (NRC) and its contractors as part of regulatory reviews of the KP-FHR design, the content herein may not be reproduced, disclosed, or used, without prior written approval of Kairos Power.

Rev	Description of Change	Date
0	Initial Issuance	June 2020
1	Addition of Non-Power Test Reactor information and response to NRC questions dated November 25, 2020	June 2021

EXECUTIVE SUMMARY

This Topical Report describes the qualification plans for structural alloys used in the safety-related systems of reactors utilizing Kairos Power Fluoride Salt-Cooled, High Temperature Reactor (KP-FHR) technology. The plans described herein are applicable to KP-FHR power reactors and non-power (test) reactors. These reactors operate near atmospheric pressure and utilize high temperature fuel and molten salt coolants to provide a high degree of passive safety.

This document describes the testing and modelling required to qualify the structural alloy materials used in the safety-related portion of the plants, i.e., the fluoride salt cooled reactor system. In the reactor system, the reactor vessel is the primary safety related component, as it serves to maintain Flibe coolant around the fuel in the reactor core. This report does not describe, nor does it apply to material qualification for non-safety related systems or components. Specifically, this report describes work to extend the ASME qualification of structural alloys to higher temperatures, to generate additional high temperature design data, and to demonstrate environmental compatibility of the structural materials. The environmental compatibility testing for the commercial power reactor is detailed in the body of the report and a limited scope test plan for the shorter-lived non-power test reactor is provided in Appendix E. Additionally, this report presents, for information, ongoing work to develop coatings and cladding and reliability and integrity management plans.

Kairos Power is requesting Nuclear Regulatory Commission review and approval of the qualification plan described in this report for metallic structural materials used in Flibe wetted areas for safety-significant high temperature components of the reactors for use by licensing applicants under 10 CFR 50 or 10 CFR 52. This includes approval of the planned testing and analyses to address the materials reliability and environmental compatibility issues via design, operation, and inspection. The results of these planned tests and analyses, along with a description of the design and inspection program will be provided in a future license application.

Table of Contents

Executive Summary.....	4
List of Abbreviations	11
1 INTRODUCTION (INFORMATION)	12
1.1 Design of the KP-FHR	12
1.1.1 Design Background.....	12
1.1.2 Design Background.....	13
1.1.3 Key Features.....	13
1.2 Regulatory Information.....	15
1.2.1 Regulations Relevant to the KP-FHR Material Qualification.....	15
1.2.2 Principal Design Criteria that are Relevant to the KP-FHR Material Qualification	16
2 Structural Alloys (INFORMATION).....	18
2.1 Background	18
2.2 Structural Alloy Selection.....	18
2.3 Industrial Experience with Alloy 316H and its Weld Filler Metals	20
2.3.1 Conventional Nuclear Reactors.....	20
2.3.2 Advanced Nuclear Reactors	20
2.3.3 Other Industrial Applications of Alloy 316	21
2.3.4 Compatibility with Molten Salts.....	22
3 AIR TESTING AND FINITE ELEMENT ANALYSEs (INFORMATION)	23
3.1 Testing Required for ASME Code Extension	23
3.1.1 Elevated Temperature Tensile Testing	24
3.1.2 Creep-Fatigue Testing	24
3.1.3 Creep-Rupture Testing	24
3.2 Testing to Facilitate NON-POWER REACTOR AND COMMERCIAL POWER REACTOR Designs....	25
3.2.1 Tensile Testing.....	25
3.2.2 Stress Relaxation Testing	25
3.2.3 Stress Dip Testing.....	25
3.2.4 Uniaxial and Notched Bar Creep Testing	26
3.2.5 Creep-Fatigue Testing	26
3.3 Air Testing to Support Potential Degradation.....	26
3.3.1 Stress Relaxation Cracking	26
3.3.2 Weld Residual Stresses	27
3.3.3 Thermal Stresses & Thermal Striping.....	28
4 COMPATIILIITY WITH FLIBE AND IRRADIATION (APPROVAL UNLESS NOTED).....	29
4.1 Review of Potential Environmental and Irradiation Issues.....	29
4.2 Environmental Compatibility	30
4.2.1 Use of the PIRT Data for NRC Licensing	30

4.2.2	Alloys and Heats to be Assessed.....	31
4.2.3	Corrosion.....	31
4.2.4	Environmentally Assisted Cracking.....	36
4.2.5	Metallurgical Effects	37
4.2.6	Irradiation Effects.....	38
5	Conclusions and Limitations	41
5.1	Conclusions	41
5.2	Limitations.....	41
6	References	42
	Table 1. Summary of Key Parameters for the Power Reactor and the Non-Power Test Reactor.....	48
	Table 2. Ranking of Structural Alloys for FHR Applications.....	49
	Table 3. Summary of Tests to Extend the ASME Qualification of ER16-8-2 to 816°C.....	50
	Table 4. Summary of Planned Tensile Tests to Support Non-Power Test Reactor Design	51
	Table 5. Summary of Planned Stress Relaxation Tests to Support Non-Power Test Reactor Design	52
	Table 6. Summary of Planned Strain Rate Change (aka 'stress dip') Tests to Support Non-Power Test Reactor Design	53
	Table 7. Summary of Uniaxial Creep Tests to Support Non-Power Test Reactor Design	54
	Table 8. Summary of Planned Notched Bar Creep Tests to Support Non-Power Test Reactor Design....	55
	Table 9. Summary of Planned Creep-Fatigue Tests to Support Non-Power Test Reactor Design.....	56
	Table 10. Summary of Potential Testing to Assess Stress Relaxation Cracking	57
	Table 11. Summary of Testing and Analysis Judged to be Warranted by the Materials PIRT Review.....	58
	Table 12. Overall Effects that will be Assessed to Develop Corrosion Rate Models	59
	Table 13. Detailed Plans for Corrosion Testing	60
	Table 14. Summary of Planned Slow Strain Rate Testing to Assess Environmentally Assisted Cracking ..	61
	Table 15. Planned Conditions for Corrosion Fatigue Crack Growth Rate and Stress Corrosion Cracking Tests	62
	Table 16. Test Conditions to Assess Creep-Rupture Performance in Flibe	63
	Table 17. Specimens Planned for Characterization to Assess Metallurgical Effects.....	64

Table 18. Target Temperature, Representative Doses, and Estimated Helium Concentrations for Post-Irradiation Tensile and Creep Testing	65
Table 19. Target Irradiation and Out of Pile Test Conditions for Post-Irradiation Creep Testing.....	66
Figure 1. DELETED	67
Figure 2. Overview of the Commercial Power Generation Reactor Heat Transport Loops with Nominal Operating Temperatures	68
Figure 3. Comparison of the Operating Pressures and Temperatures of Selected Conventional and Advanced Reactor Designs.....	69
Figure 4. Comparison of the Operating Conditions of Alloy 316H in the KP-FHR (blue box) with Oil & Gas Refinery Components and Existing Creep Rupture Data	70
Figure 5. DELETED	71
Figure 6. Illustration of the Environmental Degradation Mechanisms Considered in the Kairos Power PIRT Review of Environmental Degradation.....	72
Figure 7. The Knowledge and Importance Rankings Used by the Expert Panel to Assess Environmental Degradation Phenomena	73
Figure 8. Summary of the PIRT Rankings	74
Figure 9. DELETED	75
Figure 10. Illustration of Slow Strain Rate Testing (SSRT) Data (left) and How the Results May Be Used to Map Out Regimes of Susceptibility to Environmentally Assisted Cracking (right)	76
Figure 11. Example Corrosion Fatigue Crack Growth Rate Data (left) and How They Will be Compared to Data Collected in Air (right) to Assess the Effect of Environment	77
Figure 12. Illustration of a Potential SCC Mechanism in Flibe (top) where Grain Boundary Cr Loss is Accelerated at a Strained Crack Tip and (bottom) Schematic SCC Growth Rate Data	78
Figure 13. Comparison of the Evolution of Irradiation Damage and Helium Generation in the KP-FHR Reactor Vessel.....	79
Figure 14. How Irradiation Affects Fracture Toughness in Austenitic Stainless Steels and Specific Data for Alloy 316 and 304 at 550°C.....	80
Figure 15. Illustration of How Strain Rate and Temperature Affect Tensile Ductility in an Austenitic Stainless Steel Irradiated to a Helium Content of ~7 at. ppm	81
Figure 16. (a) Normalized Creep Strength After Irradiation (Ratio of Irradiated Stress to Unirradiated stress to Reach the Same Average Creep Life) (b) Normalized Creep Ductility After Irradiation (Ratio of Irradiated Ductility to Unirradiated Ductility at the Same Stress	82

Figure 17. Variable Corrosion Rate of Alloy 316 Stainless Steel with Time (top) and The Strong Benefit of Be Addition (Redox Control) (bottom).....	83
Figure 18. Data of Zheng et al, Illustrating the Effect of Graphite on the Corrosion Depth (top) and Corrosion Rate of Alloy 316L in Flibe at 700°C (right)	84
Figure 19. Examples of Weld Pad Buildups (top) and A V-Groove Weld (bottom) used to Fabricate Test Samples.....	85
Figure 20. Comparison of the Composition of Heat 578409 (+ symbols) Relative to the ASME Code Specification (dashed lines, from Section II. 2017).	86
Figure 21. Selected Creep-Rupture Data for ER16-8-2 Weld Filler Metal Compared to the Best Estimate Prediction and Confidence Bounds.....	87
Figure 22. Comparison of Selected Base Metal and Weld Metal Tensile Data.....	88
Figure 23. Weld Designs that Minimizes the Risk of Stress Relaxation Cracking.....	89
Figure 24. Notch Bar Testing Used to Assess the Susceptibility of Alloy 316H Stainless Steel to Stress Relaxation Cracking.....	90
Figure 25. Potential Location of the CCS Relative to the Reactor Vessel.....	91
Figure 26. Predicted Grain Boundary Diffusion Rate	92
Figure 27. Schematic Illustration of a Rotating Cage Loop (RCL) Corrosion Testing System (left) and an Operational RCL System (right).....	93
Figure 28. Example of Fluoride Salt Compositional Analysis	94
Figure 29. The Time-Temperature-Transformation Diagram for Alloy 316H	95
Figure 30. Calculated LiF-BeF ₂ Phase Diagram Against Experimental Data.....	96
Figure 31. Calculated Multicomponent Phase Diagram with Superimposed Log (p(HF))	97
Figure 32. Schematic of the In-Situ Mechanical (ISM) Testing Systems (left) and an Operational ISM Running a Slow Strain Rate Test in FLiNaK Salt (right).....	98
Figure 33. Example Fitting and Extrapolation of Degradation Rate	99
APPENDIX A. Coatings, Cladding, and Tritium Management	100
Appendix A Table 1. Comparison of Selected Coatings and Cladding of Interest to the KP-FHR	102
APPENDIX B. Inspection and Aging Management	103
APPENDIX C. DETAILS OF THE CORROSION Data Analysis.....	105

Appendix C Figure 1. Example of How a Corrosion Coupon was Sectioned (left) and Corresponding Compositional Maps for Iron, Chromium, and Nickel	107
Appendix C Figure 2. The Corrosion Data of Alloy 316L in Flibe of Zheng (Pink Squares) Compared to Example Data at Three Different Temperatures.....	108
Appendix C Figure 3. Example of How Corrosion Data May be Fit and Extrapolated to Times Out to 20 years.....	109
Appendix C Figure 4. Example of How the Baseline Corrosion Model May be Compared to a Separate Effects Test to Determine a Factor of Improvement	110
APPENDIX D. DELETED	111
APPENDIX E. TESTING AND ANALYSIS REQUIREMENTS for THE NON-POWER TEST REACTOR	112
Environmentally Assisted Cracking Testing	114
Metallurgical Effects (previously 'Other')	114
Irradiation Effects.....	115
Conclusions for the Non-Power Test Reactor.....	116
Appendix E Table 1. Areas to Address Based on the KP-FHR Metallic Materials Qualification Plan	117
Appendix E Table 2. Changes to the Corrosion Testing Plan for the Non-Power Test Reactor	118
Appendix E Table 3. Summary of Planned Slow Strain Rate Tests to Assess the Potential for Environmentally Assisted Cracking on both the Non-Power Test Reactor and Power Reactor.....	119
Appendix E Table 4. Summary of Planned Corrosion Fatigue and Stress Corrosion Cracking Tests to Assess the Potential for Environmentally Assisted Cracking in the Non-Power Test Reactor and Power Reactor	120
Appendix E Table 5. The Environmental Creep Tests that are Eliminated for the Non-Power Test Reactor 121	
Appendix E Table 6. Testing to Assess Stress Relaxation Cracking that are Delayed or Eliminated for the Non-Power Test Reactor	122
Appendix E Table 7. Summary of the Proposed Changes to Metallurgical Effects Tests for the Non-Power Test Reactor	123
Appendix E Table 8. Proposed Elimination of the Irradiation Embrittlement Testing Plan for the Non-Power Test Reactor.....	124
Appendix E Table 9. Proposed Elimination of the Irradiated Creep Tests for the Non-Power Test Reactor 125	
Appendix E Figure 1. Good Fit Between a Grain Boundary Diffusion-Based Corrosion Model for Chromium Loss (solid lines) and the Corrosion Data for Alloy 316L in Flibe	126

APPENDIX F. Certified Material Reports	127
Appendix F Figure 1. Material Certification Report for Alloy 316H Plate	127
Appendix F Figure 2. Overcheck of the Composition of the Alloy 316H Plate.....	128
Appendix F Figure 3. Material Certification Report for the ER16-8-2 Weld Wire	129
Appendix F Figure 4. Material Certification Report for Second Heat of ER16-8-2	130
Appendix F Figure 5. Material Certification Report (tentative) for a Third Heat of ER16-8-2	131

LIST OF ABBREVIATIONS

Acronym	Definition
ASME	American Society for Mechanical Engineers
ASTM	American Society for Testing and Materials
BWR	Boiling Water Reactor
CFR	Code of Federal Regulations
DPA	Displacements per Atom
DOE	Department of Energy
EAC	Environmentally Assisted Cracking
FHR	Fluoride Salt-Cooled High Temperature Reactor
FSAR	Final Safety Analysis Report
HFIR	High Flux Isotope Reactor
IASCC	Irradiation-Assisted Stress Corrosion Cracking
IGSCC	Intergranular Stress Corrosion Cracking
KP-FHR	Kairos Power Fluoride Salt-Cooled, High Temperature Reactor
LWA	Limited Work Authorization
LWR	Light Water Reactors
MANDE	Monitoring and Non-Destructive Examination
MHTGR	Modular High Temperature Gas Reactor
MSR	Molten Salt Reactor
MSRE	Molten Salt Reactor Experiment
NRC	Nuclear Regulatory Commission
OFHC	Oxygen-Free, High-Conductivity
ORNL	Oak Ridge National Laboratory
PDC	Principal Design Criteria
PIRT	Phenomena Identification and Ranking Table
PSAR	Preliminary Safety Analysis Report
PWR	Pressurized Water Reactor
RCL	Rotating Cage Loop
RG	Regulatory Guide
RIM	Reliability and Integrity Management
SCC	Stress Corrosion Cracking
SFR	Sodium-Cooled Fast Reactor
SSC	Structure, System, or Component
SSRT	Slow Strain Rate Testing
TRISO	Tri-Structural Isotropic

1 INTRODUCTION (INFORMATION)

Kairos Power LLC (Kairos Power) is pursuing the design, licensing, and deployment of reactors based on Fluoride Salt-Cooled, High Temperature Reactor technology. To construct these reactors, Kairos Power will rely on the use of qualified high temperature metallic structural materials in selected applications. The materials qualification program relies on both materials testing and modeling to ensure the performance of the safety-related metallic structural materials. This report details the approach for safety-related metallic structural materials qualification in Flibe wetted areas for the KP-FHR consistent with American Society of Mechanical Engineers (ASME) Section III Division 5 (Rules for Construction of Nuclear Power Plant Components, High Temperature Reactors) requirements.

The structural alloys for use in the safety-related Flibe wetted areas of the reactor were selected considering the commercial availability and if the material is qualified for use via ASME Section III Division 5. These rules for construction require demonstration of the environmental compatibility of the structural materials. A Phenomena Identification and Ranking Table (PIRT) type process as described in Regulatory Guide (RG) 1.203, "Transient and Accident Analysis Methods" (Reference 1) was used to identify significant degradation phenomena and to develop the testing and modelling qualification presented in this report.

The design of the safety-related Flibe wetted areas of the reactor does not require the application of cladding or coatings [[

]]. If coatings or cladding are used in the safety-related

Flibe wetted portions of the reactor, their use in the design will be in a manner consistent with ASME Code rules. For example, ASME Section III, Division 5, Subsection HB, Subpart B for structural load carrying Class A materials (Reference 2).

This report also presents an overview of a Reliability & Integrity Management (RIM) Program for information. The RIM program is an integral part of nuclear component life cycle management. A new approach for RIM of high temperature reactors is being developed by ASME Section XI Division 2. Article VII-4 of the Code has been reserved for molten salt reactors (and presumably solid fueled FHR designs) and is expected to be published in July 2021. A RIM program will be described as part of the operating licensing application for a KP-FHR.

1.1 DESIGN OF THE KP-FHR

To facilitate NRC review and approval of this report, design features considered essential to the KP-FHR technology are provided in this section. These key features are not expected to change during the ongoing detailed design work by Kairos Power and provide the basis to support the safety review. Should fundamental changes occur to these design features or revised regulations be promulgated that affect the conclusions in this report, such changes will be reconciled and addressed in future license application submittals.

1.1.1 Design Background

The KP-FHR is a U.S.-developed Generation IV advanced reactor technology. In the last decade, U.S. National Laboratories and Universities have developed conceptual Fluoride Salt-Cooled High-Temperature Reactor (FHR) designs with different fuel geometries, core configurations, heat transport systems, power cycles, and power levels. More recently, the University of California at Berkeley developed the Mark 1 pebble-bed FHR, incorporating lessons learned from the previous decade of designs

(Reference 3). Kairos Power has built on the foundation laid by Department of Energy (DOE)-sponsored, University-led Integrated Research Projects to develop the KP-FHR. Although not intended to support the findings necessary to approve this report, additional design description information is provided in the “Design Overview of the Kairos Power Fluoride Salt-Cooled, High Temperature Reactor” Technical Report (Reference 4).

1.1.2 Design Background

Kairos Power is developing both a non-power test reactor and a commercial power generation reactor based on KP-FHR technology. The operating parameters discussed in this topical report will apply to both reactor classes. The non-power test reactor will operate at lower power level and potentially lower temperatures than the power reactor. For the purposes of the metallic material qualification, the operating parameters for the power reactor are considered to bound those that will exist in the test reactor. One difference that will have a bearing on data needed to qualify the metallic material is the expected lifetime of the safety-related flibe wetted components in the reactor. The non-power reactor component lifetime is expected to be limited to 10 years, while the component lifetime in the power reactor will be on the order of [[]] or more. Appendix E contains the specific details of metallic materials qualification for the non-power reactor. The key features of the power and non-power reactors are compared in Table 1.

1.1.3 Key Features

The KP-FHR technology integrates key design features and material choices into a physically compact, intrinsically safe, high temperature reactor which will be built with existing, industrially proven materials. Key design features of the KP-FHR include the use of high temperature fuel, high boiling point molten salt coolants, and low-pressure operation. This combination of the Tri-Structural Isotropic (TRISO) particle fuel, stable high boiling temperature fluoride salt coolant, and low operating stresses results in a robust reactor design with intrinsic passive safety. Notably, the reactor vessel is expected to see <0.1 dpa for the lifetime of both the non-power and power reactors.

The fuel in the KP-FHR is based on the TRISO high-temperature fuel. TRISO fuel is a carbon matrix coated particle fuel, originally developed for high-temperature gas-cooled reactors, in a pebble fuel element. Coatings on the particle fuel provide retention of fission products to temperatures approaching 1600°C. The primary coolant that is used in safety-related systems is a mixture of lithium fluoride (LiF) and beryllium fluoride (BeF₂) salts in a ratio of approximately 2:1. This F-Li-Be based salt, i.e., ‘Flibe’ has been proven as an effective nuclear coolant in the Molten Salt Reactor Experiment (MSRE) program and the operation of the MSRE nuclear reactor (Reference 74). Furthermore, there has been significant research into the stability and compatibility of Flibe in nuclear applications since the operation of the MSRE. The KP-FHR is a low-pressure reactor which operates with a modest overpressure (~0.2 MPa or 2 atm) in the reactor vessel head space to minimize contamination of the primary coolant. The low-pressure operation and associated low operating stresses are another key design feature of the KP-FHR. Low operating stresses help enable the use of conventional metallic structural materials and provides significant margin against high temperature failure modes such as creep-rupture.

1.1.3.1 Heat Transport Systems

Both the non-power test reactor and the commercial power generation reactor are expected to include at least two heat transfer loops. A primary loop contains Flibe and maintains cooling in the core. Another heat transfer loop(s) removes heat from the primary system during normal operations for heat rejection

(test reactor) or power generation (power reactor). Figure 2 shows two heat transport loops for the power reactor and the operating temperature range (550-650°C). For both the non-power and power reactor, the hot leg of the primary heat transport loop is anticipated to operate up to 650°C and the cold leg returns the Flibe to the reactor vessel at 550°C.

The KP-FHR design includes two decay heat removal systems. A system for providing decay heat removal is used following normal shutdowns and a separate passive decay heat removal system, [[

]] removes decay heat in response to postulated events. Note that the passive decay heat removal system does not rely on electrical power to accomplish its safety function.

1.1.3.2 Containment Approach

The KP-FHR design uses a functional containment approach, like the Modular High Temperature Gas-Cooled Reactor (MHTGR) rather than a low-leakage, pressure-retaining containment structure that is typically used for light water reactors (LWRs). The KP-FHR functional containment safety design objective is to meet 10 CFR 50.34 (10 CFR 52.79) offsite dose requirements at the plant's exclusion area boundary with margin. A functional containment is defined in RG 1.232, "Guidance for Developing Principal Design Criteria for Non-Light Water Reactors" as a "barrier, or set of barriers taken together, that effectively limit the physical transport and release of radionuclides to the environment across a full range of normal operating conditions, anticipated operational occurrences, and accident conditions. RG 1.232 includes an example design criterion for the functional containment (MHTGR Criterion 16). As also stated in RG 1.232, the NRC has reviewed the functional containment concept and found it "generally acceptable," provided that "appropriate performance requirements and criteria" are developed. The NRC staff has developed a proposed methodology for establishing functional containment performance criteria for non-LWRs, which is presented in SECY-18-0096, "Functional Containment Performance Criteria for Non-Light-Water-Reactors". This SECY document has been approved by the Commission.

The functional containment approach for the KP-FHR is to control radionuclides primarily at their source within the coated fuel particle under normal operations and accident conditions without requiring active design features or operator actions. The KP-FHR design relies primarily on the multiple barriers within the TRISO fuel particles and fuel pebble to ensure that the dose at the site boundary (from postulated accidents) meets regulatory limits. Additionally, in the KP-FHR (but not in MHTGR designs), the molten salt coolant serves as an additional barrier providing retention of fission products that could escape the fuel particle and fuel pebble barriers. This additional retention barrier is a key feature of the enhanced safety and reduced source term in the KP-FHR. To enable fission product retention of the Flibe coolant, the reactor vessel must retain the coolant around the fuel pebbles. Thus, the reactor vessel is considered to be a safety-related structure. [[

]]

1.1.3.3 Reactor Vessel

The anticipated design of the KP-FHR reactor vessel is based on a vertical cylinder with bottom and top heads. The vessel is expected to be constructed from materials that are qualified by the ASME Section III. The reactor vessel serves as part of the reactor coolant boundary and supports and interfaces with other systems such as rod control, pebble handling, and heat removal systems. The reactor vessel will be designed to withstand the operational loads imparted on it by the core structures, fuel, and coolant.

Additionally, the reactor vessel will be of sufficient strength and resiliency to withstand off-nominal conditions required by ASME Section III Division 5 Level B, C, and D Service Conditions (Reference 37).

[[

]]

1.2 REGULATORY INFORMATION

1.2.1 Regulations Relevant to the KP-FHR Material Qualification

The KP-FHR is anticipated to be licensed under Title 10 of the Code of Federal Regulations (10 CFR) using a licensing pathway provided in Part 50 or Part 52. Applicants for construction permits for facilities licensed under 10 CFR 50 are required to provide a Preliminary Safety Analysis Report (PSAR), which provides a safety assessment of the facility in accordance with 10 CFR 50.34(a). Applicants for a Limited Work authorization (LWA) are required to submit a safety analysis that meets 10 CFR 50.34 for the scope of the LWA per 10 CFR 50.10(d)(3)(i). Subsections within 10 CFR 50.34(a) relevant to the requirement to describe design characteristics of the KP-FHR high temperature materials are listed below (note these are required to be updated as part of the operating license application in the Final Safety Evaluation Report (FSAR) per 10 CFR 50.34(b)(4)):

50.34(a)(1)(ii)(B) The extent to which generally accepted engineering standards are applied to the design of the reactor.

50.34(a)(1)(ii)(C) The extent to which the reactor incorporates unique, unusual, or enhanced safety features having a significant bearing on the probability or consequences of accidental release of radioactive materials.

50.34(a)(2) A summary description and discussion of the facility, with special attention to design and operating characteristics, unusual or novel design features, and principal safety considerations.

50.34(a)(3)(ii) The preliminary design of the facility including the design bases and the relation of the design bases to the principal design criteria.

Similarly, applicants for combined licenses for facilities licensed under 10 CFR 52 are required to provide a FSAR which provides a safety assessment of the facility in accordance with 10 CFR 52.79. Subsections relevant to the design and performance of high temperature materials are as follows:

52.79(a)(2) A description and analysis of the structures, systems, and components of the facility with emphasis upon performance requirements, the bases, with technical justification therefor, upon which these requirements have been established, and the evaluations required to show that safety functions will be accomplished. It is expected that reactors will reflect through their design, construction, and operation an extremely low probability for accidents that could result in the release of significant quantities of radioactive fission products. The descriptions shall be sufficient to permit understanding of the system designs and their relationship to safety evaluations. Items such as the

reactor core, reactor coolant system, instrumentation and control systems, electrical systems, containment system, other engineered safety features, auxiliary and emergency systems, power conversion systems, radioactive waste handling systems, and fuel handling systems shall be discussed insofar as they are pertinent.

52.79(a)(ii) The extent to which generally accepted engineering standards are applied to the design of the reactor.

52.79(a)(2)(iii) The extent to which the reactor incorporates unique, unusual, or enhanced safety features having a significant bearing on the probability or consequences of accidental release of radioactive materials.

52.79(a)(2)(iv) The safety features that are to be engineered into the facility and those barriers that must be breached as a result of an accident before a release of radioactive material to the environment can occur. Special attention must be directed to plant design features intended to mitigate the radiological consequences of accidents.

52.79(a)(4)(ii) The design of the facility including the design bases and the relation of the design bases to the principal design criteria.

Similar requirements to these are also included in 10 CFR 52.47 for Standard Design Certifications; 10 CFR 52.137 for Standard Design Approvals; and 10 CFR 52.157 for manufacturing licenses.

The use of metallic structural materials in high temperature Flibe salt environments is considered to represent a new and unique feature not typical of existing licensed light water reactor designs. The design and thermophysical properties of the KP-FHR reactor coolant enhances the safety of operations and reduces the probability of events [[

]]. The design and thermophysical properties of the KP-FHR reactor coolant also provides additional functional containment protection, beyond that provided by the TRISO fuel particle, by absorbing fission products that escape the TRISO protective layer. This design feature reduces the probability of accidental release of radioactive materials. The specification limits and thermophysical properties of the reactor coolant for the KP-FHR are provided in the Kairos Power Topical Report, "Reactor Coolant for the Kairos Power Fluoride Salt-Cooled High Temperature Reactor" (Reference 6). This report describes the qualification and testing methods for the metallic structural materials in the high temperature Flibe salt environments for use in the Flibe wetted areas containing safety-related high temperature components of the KP-FHR. As such, qualification of these materials using the methodology described in this report supports conformance, in part, to 10 CFR Part 50, Sections 50.34(a)(1)(ii)(C), 50.34(a)(2), 10 CFR 50.34(b)(4); and to 10 CFR Part 52, Sections 52.79(a)(2) and equivalent regulations in 52.47, 10 CFR 52.137, and 10 CFR 52.157.

1.2.2 Principal Design Criteria that are Relevant to the KP-FHR Material Qualification

Facilities licensed under 10 CFR Part 50 are also required to describe Principal Design Criteria (PDC) in their safety analysis reports supporting a construction permit and operating license application as described in 10 CFR 50.34(a)(3)(i). Likewise, applicants for standard design certifications, combined licenses, standard design approvals, and manufacturing licenses must include the PDC for a facility as described in 10 CFR 52.47(a)(3)(i), 10 CFR 52.79(a)(4)(i), 10 CFR 52.137(a)(3)(i), and 10 CFR 52.157(a).

The PDC for the KP-FHR have been established in the Kairos Power Topical Report, “Principal Design Criteria for the Kairos Power Fluoride Salt Cooled High Temperature Reactor” (Reference 7). The specific PDC in this report, which rely on or credit the design and performance of high temperature metallic structural materials include PDCs 14 and 31. These PDCs are discussed below.

The design and performance of high temperature metallic structural materials is relative to demonstrating conformance to PDC 14 because the materials used in the KP-FHR must ensure that they do not fail. The PDC states:

The safety-significant elements of the reactor coolant boundary are designed, fabricated, erected, and tested such that they have an extremely low probability of abnormal leakage, of rapidly propagating failure, and gross rupture.

The design and performance of high temperature metallic structural materials is relative to demonstrating conformance to PDC 31 because the materials used in the KP-FHR must ensure that they are not unduly stressed under operating, maintenance, testing, and postulated accidents. PDC 31 states:

The safety significant elements of the reactor coolant boundary are designed with sufficient margin to ensure that when stressed under operating, maintenance, testing, and postulated accident conditions, (1) the boundary behaves in a nonbrittle manner and (2) the probability of rapidly propagating fracture is minimized. The design reflects consideration of service temperatures, service degradation of material properties, creep, fatigue, and other conditions of the boundary material under operating, maintenance, testing, and postulated accident conditions, and the uncertainties in determining: (1) material properties, (2) the effects of irradiation and coolant composition, including contaminants and reaction products, on material properties, (3) residual, steady-state, and transient stresses, and (4) size of flaws.

Corrosion of structural materials is an important consideration for maintaining the integrity of the safety-significant portions of the reactor coolant boundary. Demonstration, through qualification, of the acceptability of the metallic structural materials used in the safety-significant portions of the reactor coolant boundary is a key element in establishing conformance to PDC 14 and PDC 31. The qualification requirements described in Sections 3 and 4 of this report (as well as Appendix E for the non-power test reactor), partially satisfy PDC 14 and PDC 31. A description of how the remaining portions of these PDC are satisfied will be provided in safety analysis reports submitted with licensing applications for the KP-FHR.

2 STRUCTURAL ALLOYS (INFORMATION)

2.1 BACKGROUND

Ductile, face-centered-cubic iron and nickel-based alloys (i.e., ‘austenitic’ alloys) are commonly used structural materials in light water reactors due to their combination of strength, toughness, and corrosion-resistance. Light Water Reactor (LWR) operation involves modest temperatures (215-345°C) but relatively high operating pressures (~7 MPa for BWR’s and 16 MPa for PWR’s). These temperatures translate into homologous temperatures (TH^1) of ~0.27-0.36 for the structural materials. These homologous temperatures are low enough such that solid state diffusion rates are slow and many degradation phenomena (e.g., alloy phase stability, creep, etc.) are of limited consequence.

Like LWR’s, the KP-FHR design intends to use iron and nickel-based alloys for metallic structural components but at higher temperatures, lower pressure, and in different environments than LWRs. Specifically, the design of safety-significant components of the KP-FHR will use austenitic alloys at homologous temperatures [[]] in both reducing and oxidizing molten salts. These higher temperatures require more consideration of high temperature material phenomena (e.g., thermal creep deformation) and, like water reactors, the molten salt coolants will require compositional control to ensure the metallic structural materials maintain resistance to corrosion and to environmentally assisted cracking. For comparison, the approximate operating pressures, and temperatures of LWR’s, high temperature gas reactors HTGR’s and sodium-cooled fast reactors (SFR’s) and the KP-FHR is given in Figure 3. As shown, the KP-FHR will operate at significantly lower pressures than the BWR’s, PWR’s and high temperature gas reactors and at comparable pressures but somewhat higher temperatures than SFR’s.

2.2 STRUCTURAL ALLOY SELECTION

The design of the KP-FHR reactor coolant boundary will be constructed from alloys qualified (or near qualification) by the ASME Code. Currently in ASME, Section III, Division 5, there are only a few alloys that are suitable for temperatures $\geq 600^\circ\text{C}$. These include the austenitic Alloys 304H, 316H, 800H, and 617. Additionally, a modified version of Hastelloy N, the DOE developed Alloy 709, and the stainless-steel weld filler metal ER16-8-2 were included in the consideration for structural alloy selection. These 7 alloys were ranked based on ten criteria:

- Status of ASME Code Qualification
- Mechanical and Physical Properties
- Experience with Molten Salts
- Experience in Nuclear Reactor Systems
- Technical Maturity
- Ability to Procure the Alloy in a Wide Variety of Product Forms
- Ease of Fabrication and Existence of a Matching Weld Filler Metal
- Environmental Compatibility of the Alloy with the KP-FHR Environments
- Degree of Regulatory Acceptance of the Alloy for use in Nuclear Systems
- Cost of the Alloy

A comparison of these rankings is provided in Table 2. As shown, the ranking for each category were assigned on a scale of 1 to 5 with a high rank (1 or a blue filled circle) being the most desirable and a low

¹ Homologous temperature is defined as the temperature of interest divided by the melting point of the pure element that that alloy is based on in absolute units.

rank (5 or an open circle) being the least desirable. A summary of the factors that influenced eliminating the other structural alloys are provided below.

Alloy 304H is similar in composition and in many attributes to Alloy 316H. However, Alloy 304H displays notably lower creep strength at high temperatures. The benefits of Alloy 304H relative to Alloy 316H are few (e.g., marginally lower cost) and do not provide compelling reasons to select this alloy over Alloy 316H. Lastly, available data indicate higher corrosion rates for Alloy 304 as compared to Alloy 316 in Flibe (Reference 34). For these reasons, 304H was eliminated from consideration in favor of the more capable Alloy 316H.

Alloy 800H is often used in high temperature applications that require corrosion resistance. However, Alloy 800H is less creep-resistant than Alloy 316H and contains higher levels of chromium (~21 wt.% Cr vs. ~17 wt.%). Higher chromium levels are undesirable for corrosion-resistance in Flibe. Furthermore, Alloy 800H does not have a matching weld filler metal but is often welded with high chromium nickel-based alloys such as EN82H. The higher nickel in Alloy 800H/EN82 relative to Alloy 316H/ER16-8-2 is less desirable due to the potential transmutation of nickel to helium, which will adversely affect irradiation embrittlement. For these reasons, Alloy 800H is ranked lower than Alloy 316H stainless steel.

Alloy 617 was recently added to ASME Section III, Division 5 and possesses superior high temperature strength and creep resistance relative to Alloy 316H. However, the alloy contains a large amount of cobalt (10-15 wt.%) which can undergo undesirable neutron activation. The high strength of Alloy 617, while desirable, is not required for the KP-FHR design. Moreover, the attractive high temperature strength can present challenges when trying to hot-form the alloy and leads to fabrication challenges. Lastly, due to the expense and limited market for Alloy 617 relative to more common alloys like Alloy 304 and Alloy 316, Alloy 617 is only commercially available in limited product forms.

Hastelloy N showed excellent corrosion-resistance in the MSRE experience but was susceptible to both tellurium embrittlement and degradation by irradiation (Reference 8 and 9). For this reason, a modified grade of Hastelloy N was considered in the rankings. However, Hastelloy N is not currently approved for use by ASME in high temperature reactors and modified grades are likely different enough composition (e.g., containing several weight % of niobium) to require a full ASME qualification effort. Furthermore, it is unclear what a suitable weld filler metal for a modified Hastelloy N would be. The lack of code qualification, lack of off-the-shelf commercial availability, and high costs associated with bringing a new alloy to market are major limitations that precluded selecting a modified grade of Hastelloy N.

Alloy 709 is an advanced stainless steel being developed by the DOE for nuclear power applications. While not ASME code qualified, this effort is in progress and to date, Alloy 709 displays a desirable combination of properties with higher creep strength than Alloy 316H as well as the potential for increased resistance to irradiation damage via alloy design. Notably, welding of Alloy 709 with a weld filler metal of the same composition indicates promising properties with weld degradation factors near 1. While the lack of current code qualification and industrial supply lowers the current ranking of this alloy, it may be considered for use in future licensing applications for the KP-FHR.

Alloy 316H and its weld filler metal ER16-8-2 possess a desirable combination of properties relative to the other candidate alloys. Alloy 316H is currently ASME code qualified, exhibits desirable mechanical properties, has demonstrated compatibility with Flibe salt, and has an extensive experience base in nuclear reactor applications. Furthermore, the alloy is technically mature with good availability, fabricability, and relatively low cost. The weld filler metal ER16-8-2 shows notable creep resistance and a

high degree of weldability with Alloy 316H. Areas that require additional work for this alloy include extending the qualification of ER16-8-2 to higher temperatures (e.g., currently in the ASME code, the filler metal is limited to 650°C in the 2017 ASME Section III code), and additional research into the corrosion and environmental compatibility of these materials in Flibe. Based on this review, Alloy 316H/ER16-8-2 were selected as the metallic structural materials for safety-related components in the KP-FHR. These alloys were used as the basis for the expert panel PIRT review described in Section 4.1 which assessed environmental compatibility in Flibe salt. The remainder of the report is limited to the use and qualification of Alloy 316H/ER16-8-2 for safety-significant components in Flibe wetted areas of the KP-FHR.

2.3 INDUSTRIAL EXPERIENCE WITH ALLOY 316H AND ITS WELD FILLER METALS

The following sections briefly describe the use of Alloy 316 in conventional nuclear reactors, advanced nuclear reactors, in non-nuclear but comparable industrial applications, and its compatibility with molten salt.

2.3.1 Conventional Nuclear Reactors

Austenitic stainless steels including Alloy 316 and Alloy 304, along with their weld filler metals, are commonly used for light water reactor internal components and corrosion-resistant cladding. Components made from these steels include fuel support structures, core barrels, flow baffle plates, and reactor vessel cladding. The low carbon variant of the alloy (i.e., the 'L' grade) is commonly used since high temperature strength is not limiting, but grain boundary chromium depletion (i.e., sensitization) is a concern. In light water reactors, grain boundary sensitization can result in intergranular corrosion and intergranular stress corrosion cracking if coolant chemistry is not maintained (e.g., if there is significant oxygen present in the coolant). However, sensitization is not detrimental to corrosion in Flibe. Flibe salt is highly reducing and corrosion-resistance does not rely on the formation of a passive oxide film but on metallic stability in the salt. For stainless steels exposed to Flibe, the primary corrosion mechanism has been established as chromium loss (usually via grain boundary diffusion) to the coolant (Reference 10 and 11). Thus, sensitized microstructures can be beneficial since lower chromium at the grain boundary results in less chromium lost via grain boundary diffusion.

In LWRs, irradiation can cause depletion of chromium and segregation of other elements at the grain boundaries of stainless steels and this combined with tensile stress can result in Irradiation-Assisted Stress Corrosion Cracking (IASCC) if the irradiation and stress levels are sufficient. For example, baffle-to-baffle bolts between the baffle plates in PWRs are susceptible to this degradation mechanism. However, the end-of-life irradiation doses for both the non-power test reactor and commercial power reactor are expected to be lower than the dose threshold for IASCC susceptibility, so IASCC is not considered a likely risk factor for the reactors' structural material components.

2.3.2 Advanced Nuclear Reactors

Austenitic stainless steels, including Alloy 316 have seen extensive experience in Sodium-Cooled Fast Reactors (SFRs) (Reference 12 and 13). In SFR's, austenitic stainless steels have been used throughout the primary plant with good experience. Analogous to corrosion in molten salt, when impurities in sodium such as oxygen and hydrogen are controlled to low levels, corrosion rates are low and are governed by alloying element solubility levels in the coolant (Reference 14).

While the nickel-based alloy Hastelloy N was chosen as the structural alloy for the MSRE construction, Alloy 304 and Alloy 316 were assessed in the MSRE program for their resistance to corrosion and to tellurium embrittlement (Reference 15, 16, and 17). In loop-type corrosion tests (i.e., tests with a hot leg and a cold leg) using Flibe salt at 650°C, these austenitic stainless steels exhibited corrosion rates $\leq 25 \mu\text{m/year}$ for short exposure times (<3000 hours) which decreased with time to $\sim 8 \mu\text{m/year}$ after 3000-9000 hours exposure (Reference 16 and 17). Furthermore, when redox control of the salt was implemented (using Be metal additions), corrosion rates at 650°C were further reduced to levels estimated as $<2 \mu\text{m/year}$ (Reference 16). While graphite can be a factor which increases corrosion rates, the data of Zheng et al., indicate this is a relatively modest $\sim 2X$ increase in corrosion rate (Reference 18).

These results indicate that corrosion will be manageable for Alloy 316 components in the KP-FHR. For example, consider a thin-walled component such as a heat exchanger tube [[

]] . Taking a reasonable, if not conservative corrosion rate of 2 microns per year (recall, Keiser et al., showed $<2 \mu\text{m/year}$ (Reference 16) for Alloy 316 at 650°C in redox controlled Flibe) for a [[]] lifetime produces chromium loss to a depth of 0.04 mm (0.0016") or $< 4\%$ of the wall thickness. It is important to note that this 0.04 mm represents a degraded layer (Cr loss), not a true reduction in wall thickness. In the chromium depleted layer, $\sim 82\%$ of the alloy remains (i.e., Alloy 316 is ~ 18 atomic % Cr).

In addition to manageable corrosion rates in Flibe salt, austenitic stainless steels also exhibit greater resistance to tellurium embrittlement (Reference 19 and 20). The mechanism of tellurium embrittlement is well understood to be a result of the nickel – tellurium intermetallic formation (Reference 15, 21, 22, 23, and 24). Given the much lower nickel content of Alloy 316 compared to Hastelloy N, this intermetallic formation is less likely and a lower risk (Reference 25). Moreover, the KP-FHR design mitigates concern for tellurium embrittlement by the use of solid fuel and redox control of the salt (Reference 6). With the very low TRISO particle failure rate demonstrated in the DOE Advanced Gas Reactor program combined with the retention of tellurium in the fuel particle (Reference 26), the concentration of tellurium in the Flibe is expected to be significantly lower than the liquid fueled MSRE. Furthermore, the use of Be additions for redox control moves the electrochemical potential of the system away from the oxidizing regime of concern (Reference 6 and 15). For these reasons, concern for tellurium embrittlement in the KP-FHR are minimal.

2.3.3 Other Industrial Applications of Alloy 316

Austenitic stainless steels, including type Alloy 316H are used in a wide variety of high temperature industrial applications due to their corrosion-resistance, generally desirable mechanical properties, and wide industrial availability of product forms (Reference 27). For example, Alloy 316H, its welds, and similar austenitic stainless steels (Alloy 347 and Alloy 321) are used extensively in oil and gas refinery applications at temperatures and time frames of relevance to the KP-FHR (Reference 28 and 29). For example, petroleum refining applications of stainless steels include crude distillation, fluid catalytic cracking, delayed coking, hydrotreating, catalytic reforming, hydrocracking, gas plant, amine plant, sulfuric acid alkylation, and sour water stripper systems.

Furthermore, Alloy 316H and its weld metals are used in other industries near the time and temperature of the KP-FHR. Figure 4 illustrates the intended operation of the KP-FHR in the blue box ([[]] at 550°C-650°C), relative to the NIMS creep database (gray box) and selected high temperature, long life oil and gas refinery (FCCU and Cyclone) components; the typical operating temperatures and service life of these components is estimated from (Reference 29 and 76). As shown, the KP-FHR is designed to operate

at somewhat lower temperature and longer times than components in the oil and gas industry. However, it is important to note that (1) there is overlap in the time/temperature ranges of experience and (2) many oil and gas components operate at higher stresses and are limited by different environmental degradation phenomena than those of the KP-FHR. For example, Fluid Catalytic Cracking Units are typically exposed severely carburizing gaseous environments that can limit component life and rapid temperature cycles which generate appreciable thermal stresses (Reference 29 and 76). Neither condition is pertinent to the KP-FHR.

2.3.4 Compatibility with Molten Salts

In reducing salts, Alloy 316 is used in the pyro-processing of spent nuclear fuels. In that technology, chloride-based salts are used to convert oxide based nuclear fuel back to their metallic form (Reference 30, 31, and 32). In pyro-processing systems, austenitic stainless steels are used as structural alloys and generally display excellent corrosion-resistance as long as the salt is relatively free from oxidizing impurities (Reference 33). In addition to these industrial applications, there are significant laboratory data to support the use of Alloy 316 as a structural alloy in molten Flibe (Reference 16, 17, 18 and 34).

Some corrosion data for Alloy 316 in Flibe salt are shown in Figure 17, which shows corrosion depth versus time from Reference 18 and weight change versus time from the work of Keiser and Devan (Reference 16). As shown, the corrosion rate decreases with exposure time, likely with the square root of time as diffusional transport of chromium in the alloy limits the corrosion rate. As shown in the data of Zheng (top plot) the corrosion rates are on the order of $\sim 80 \mu\text{m}/\text{year}$ at short exposure times ($\sim 1000 \text{ hours}$) and decrease with the square root of time ($\sim 21 \mu\text{m}/\text{year}$ at 6000 hours). Additionally, the work of Keiser shows the significant benefit of Beryllium metal additions, which effectively scavenge oxidizing impurities and reduce corrosion rates.

Austenitic stainless steel is also compatible with Flibe and graphite as shown by the work of Zheng et al. (Reference 18). Those researchers performed 1:1 experiments with and without graphite in Flibe at 700°C and showed about a modest increase in corrosion depth with graphite Figure 18 – top plot). Using the Reference 18, data to compare predicted corrosion rates versus time, indicates graphite increases the corrosion rate approximately 2x (Reference 18). One way in which graphite likely increases the corrosion rate is by reaction with metallic chromium in the salt to form chromium rich carbides. Reaction of chromium ions in the salt to form carbides likely act to decrease the surface concentration of chromium and drive solid state diffusion. Note that in the corrosion testing programs proposed for the commercial power generation reactor and non-power test reactor, the test systems will incorporate large surface areas of graphite to capture these effects as detailed in Section 4.2.3.1.

3 AIR TESTING AND FINITE ELEMENT ANALYSES (INFORMATION)

For the design and licensing of KP-FHR reactors to the ASME code, high temperature material property data and subsequent analyses are desired. These testing and analysis efforts can be grouped as: (1) testing to extend the code qualification of ER16-8-2 weld metal up to [[]] to match the current qualification of Alloy 316H base metal and (2) testing and analyses required to support novel, high temperature design methods including elastic-plastic and inelastic design per the ASME Section III Division 5. [[

]]

3.1 TESTING REQUIRED FOR ASME CODE EXTENSION

ER16-8-2 weld filler metal is currently qualified up to 650°C in the ASME code while Alloy 316H is qualified to 816°C (Reference 37). The KP-FHR reactor vessel operates at approximately 550°C during nominal operations but could experience temperatures up to [[]] for short durations during postulated events. Thus, an extension of the ASME Section III code qualification for ER16-8-2 up to [[

]]. Mechanical testing of weldments will be required as described in the following paragraphs to develop a Code Case introducing stress rupture factors for Alloy 316 weldments with ER16-8-2 filler metal for temperatures between 650°C and [[]] .

The types of mechanical testing that are necessary to develop a Code Case for extending the stress rupture factors for Alloy 316 weldments with ER16-8-2 filler metal are described in ASME Section III Division 5, Non-Mandatory Appendix Y (Reference 37). The methods of testing that are required for such weldments as specified in Appendix Y are the ASTM E21 Elevated Temperature Tensile Testing, ASTM E2714 Creep-Fatigue Testing, and ASTM E139 Creep-Rupture Testing. In order to meet those requirements, the planned testing is detailed in Table 3 where the number in parentheses (X) indicates the number of test samples to be tested at that condition. i.e. (2) = two replicate tests.

The welds to support these tests have been fabricated utilizing Alloy 316H base metal² and ER16-8-2 weld filler metals, and the gas-tungsten-arc welding process. The Certified Material Reports for these materials are provided in Appendix F and Figure 20 shows that the composition of the weld filler metal (Heat 578409) is within ASME specifications. Two types of welds have been fabricated to support testing: (1) weld pad buildups and (2) v-groove weldments that use Alloy 316H siderails. Examples of these welds are provided in Figure 19. Note that the proposed Code Case to extend use of ER16-8-2 up to [[]] will be based on testing of a single heat (Heat # 578409 Lot YT0384) whose material certification is provided in Appendix F. This use of a single heat of material for a code case is consistent with ASME guidelines as described in HBB-Y-2300 which refers to ASME Section II, Part D, Appendix 5-1500. This article requires "...(2) creep-rupture data for weldments made with one lot of consumables for each process intended to be used with the new base material." The scope of the Code Case will limit the high temperature

² Note that all weld metal samples that are machined from weld pad buildups used Alloy 316L/316 base plates. The use of that material is appropriate since the samples machined far (>0.5") from the weld/base metal interface to mitigate any dilution of the weld metal composition. For samples that contain the base metal (e.g., cross-weld samples, other heat affected zone samples, the Alloy 316H plate was used.

applications to the Gas Tungsten Arc Welding (GTAW) process, which is the process used for fabricating the test specimens. Therefore, testing of a single heat of GTAW filler metal is sufficient to satisfy the ASME requirement.

Furthermore, these data will be assessed against larger sets of test data that encompass several heats of material to establish appropriate statistical confidence limits on the code case data. For example, a large database of ER16-8-2 weld metal was analyzed by ASME to develop a Larson Miller parameter equation for creep performance at temperatures up to 1200°F as described in ASME STP-PT-077 (Reference 40). A comparison of the ASME STP-PT-077 best estimate (solid) line and bounds (dashed lines) is given in Figure 21 which includes all available ER16-8-2 creep rupture data that has been found to date.

3.1.1 Elevated Temperature Tensile Testing

Elevated Temperature Tensile Testing will be performed per ASTM E21 on all-weld-metal and cross-weld specimens at temperatures between 650°C and [[]] (1200°F – [[]]) at intervals of 38°C (100°F). These tests will determine the 0.2% yield strength, ultimate tensile strength, % elongation and % reduction in area at each temperature. Additionally, the strength of the ER16-8-2 all-weld-metal at each temperature will be used to establish the creep-rupture and creep-fatigue test stresses. Note that preliminary data from these tests are available and are shown below in Figure 22. As shown, this data is in good agreement with literature data on ER16-8-2 filler metal.

3.1.2 Creep-Fatigue Testing

Nonmandatory Appendix HBB-T of Section III, Division 5 provides a means to assess creep-fatigue of base metals, but it does not provide a dedicated means to assess creep-fatigue of weldments (Reference 37). Instead, the creep-fatigue analysis for base metals is applied to areas with welds and conservative restrictions are applied as follows (see HBB-Y-3400 of Reference 37);

“(a) limiting the inelastic accumulated strains to one-half the allowable strain limits for the base metal

(b) limiting the allowable fatigue at weldments to one-half the design cycles allowed for the base metal

(c) reducing the allowable creep rupture strength at weldments to a fraction of the base metal value through the weld strength rupture factor when determining time-to-rupture.”

Creep-Fatigue testing per ASTM E2714 of all-weld-metal and of cross-weld specimens is performed only to verify the adequacy of the HBB-T treatment of weldments (Reference 38). If the restrictions specified in HBB-Y-3400 bound the ASTM E2714 creep-fatigue test data, then the Non-mandatory Appendix HBB-T analysis procedures for base metal with specified restrictions for welds will have been determined to be adequate for creep-fatigue analysis of welds.

3.1.3 Creep-Rupture Testing

Creep-Rupture tests will be performed in accordance with ASTM E139 (Reference 39). The time, temperature and load conditions for the creep-rupture tests are derived from design Service Level conditions. ASME Section III Division 5 HBB-Y-2200 allows creep-rupture curves to be extrapolated up to

a factor of five from the maximum creep-rupture test duration. The maximum operating service time at each temperature is therefore divided by 5x to determine the approximate maximum test duration to assess the component life. For example, for a 100,000-hour service lifetime, a minimum test duration of 20,000 hours is sufficient to bound the operating life. The test duration and temperature can then be inserted into the appropriate creep correlation (e.g., the Larson-Miller model) to estimate the test load that will be required to produce specimen rupture at each specified time and temperature combination (Reference 40).

Testing will be performed on both all-weld-metal ER16-8-2 specimens as well as on cross-weld specimens. The rupture strength of the weld metal will be divided by the rupture strength of the base metal at each time and temperature combination to determine proposed stress rupture factors. An ASME Code balloting plan will be developed and the proposed rupture factors and supporting data will be presented to the relevant ASME Code Committees for review and approval. Progress on this extension is presently being tracked through ASME Codes & Standards Record #19-2745. Once the Code Case has been approved by ASME, then it will be presented to the NRC for approval. Once approved by the NRC then the stress rupture factors at the higher temperatures will be used in the same manner as those at the lower temperatures to determine the allowable stresses for specific temperature and time durations.

3.2 TESTING TO FACILITATE NON-POWER REACTOR AND COMMERCIAL POWER REACTOR DESIGNS

To facilitate design via the ASME Section III, Division 5, additional test data are required to calibrate and validate ASME design methodologies. A testing program focused on the commercial power reactor design was presented in Table 3. The testing program contained in Appendix E is modified to support the non-power design. Essentially, there are six types of tests required for Alloy 316H stainless steel model calibration and validation, all conducted in air: (1) tensile tests, (2) stress relaxation tests, (3) strain rate change tests (aka ‘stress dip’ tests), (4) uniaxial creep rupture, (5) notched bar creep rupture testing (aka ‘3D creep tests’) and (6) creep-fatigue testing. The latest version of the high temperature air testing plan introduces a color code aimed at indicating the priority level of each test: green tests must be performed first, then blue tests and, finally, grey tests.

3.2.1 Tensile Testing

[[

]]

3.2.2 Stress Relaxation Testing

[[

]]

3.2.3 Stress Dip Testing

[[

]]

[[

]]

3.2.4 Uniaxial and Notched Bar Creep Testing

[[

]]

3.2.5 Creep-Fatigue Testing

Creep-fatigue tests to support non-power test reactor design are listed in Table 9. [[
]]

3.3 AIR TESTING TO SUPPORT POTENTIAL DEGRADATION

As part of the Phenomena Identification Ranking Table (PIRT) process detailed in Section 4.1, some degradation phenomena (or factors that influence degradation phenomena) that are primarily driven by temperature were identified. These were: (1) degradation via stress relaxation cracking, (2) weld residual stresses, (3) other thermal stresses from operation, and (4) thermal striping. Since those issues can be addressed via testing in air (and/or via modelling), they are addressed below.

3.3.1 Stress Relaxation Cracking

Cracking of austenitic stainless steels in the temperature range (approximately 500-700°C), aka ‘stress relaxation cracking’ has been a concern at since the 1950’s (Reference 77, 78, and 79). In general, alloys of greatest concern have been the stabilized grades 347 and 321 (Reference 77, 78, 80, and 81) although types 304 and 316 stainless steel can be susceptible under conditions which produce high triaxial stresses (Reference 78, 79, 82, 83 and 84) as noted by recent work by Spindler et al. (Reference 85, 86, 87, 88 and 89).

While stress relaxation cracking of weld metal has been reported in Chrome-Moly steel and 347 weld metal (where Nb(C,N) precipitation leads to susceptibility), types 16-8-2 and 316 weld filler metals are noted for their resistance (Reference 78 and 79). To date, a literature search has not revealed any reported cases of reheat or stress relaxation cracking occurring in ER16-8-2 weld metal. Instead, the concern for Alloy 316H / ER16-8-2 appears to be limited to the heat affect zone and in components that are subjected to appreciable triaxial stress (Reference 79, 87, 89 and 90).

Several approaches are used to mitigate the risk of stress relaxation cracking. These include:

- The use of Alloy 316H base metal, which is noted to be more resistant to stress relaxation cracking than the stabilized grades, as well as the use of ER16-8-2 weld filler metal, which has not been observed to exhibit stress relaxation cracking.
- Design of welds and application of welding processes and parameters which are resistant to stress relaxation cracking. Lower triaxial stresses are known to be beneficial for decreasing the risk or

severity of stress relaxation cracking. For example, the bottom head to shell weld utilizes a machined weld preparation to move the weld joint from the notch formed by the shell / bottom head interface up into the shell which minimizes the triaxial stresses (Figure 23).

- Developing the capability to model weld residual stresses and to better assess the risk of any weld joints for stress relaxation cracking if needed, and
- If needed, conducting tests to quantitatively assess the susceptibility of Alloy 316H to stress relaxation cracking.³

The testing proposed to assess stress relaxation cracking is summarized in Table 10. These tests follow the work of Spindler et al., who have used notched tensile bars to assess the effects of triaxiality and temperature on susceptibility to stress relaxation cracking (Reference 46). As shown in Table 10, tests will be conducted on Alloy 347 to serve as a baseline for susceptibility and then compared to the response of Alloy 316H as well as Alloy 316H plus a post weld heat treatment.

[[

]]

[[

]]

3.3.2 Weld Residual Stresses

Weld residual stresses are known to influence some environmental degradation phenomena like stress corrosion cracking. [[

]]

³ Note that while in the original issue of this report these tests were proposed for approval, additional understanding of this phenomenon as well as design changes to the component of interest (specifically separating the vessel to lower head weld from the stress concentration feature at that joint) are judged to remove this potential degradation mechanism. Additional justification for eliminating these tests is presented in APPENDIX E.

3.3.3 Thermal Stresses & Thermal Striping

[[

]]

4 COMPATIBILITY WITH FLIBE AND IRRADIATION (APPROVAL UNLESS NOTED)

As noted above, Alloy 316H is already an acceptable material for use in high temperature reactor applications in ASME Section III. However, the code requires demonstration of the environmental and irradiation compatibility of the structural materials. For the KP-FHR safety-related systems, the environments of interest include high temperature air (external to the system) and molten Flibe salt (internal to the system), with exposure to neutron irradiation.

4.1 REVIEW OF POTENTIAL ENVIRONMENTAL AND IRRADIATION ISSUES

Due to the breadth and complexity of environmental issues, an expert panel consisting of experts from national laboratories, universities and consultants was convened to assess potential environmental issues for Alloy 316H / ER16-8-2 in each of the KP-FHR heat transport loops. This review utilized a process based on the Phenomena Identification and Ranking Table (PIRT) methodology in NRC Regulatory Guide 1.203. Only the environmental degradation issues pertinent to potential safety-related components (exposed to Flibe and air) are summarized in this report. Component materials degradation considerations are summarized in Figure 6, which presents the Venn Diagram for the Material – Stress/Strain – Environment degradation phenomena of concern for the expert panel.

In total, there were 23 degradation phenomena assessed by the expert panel in 7 unique systems, structures, and components (SSC's). This resulted in 198 scenarios assessed by the expert panel to start, with ten scenarios added during the PIRT for 208 total rankings. Each scenario was ranked based on its importance (high, medium, low) and the degree of knowledge (high, medium, low). The PIRT rankings are shown schematically in Figure 7. Phenomena with high importance and low knowledge are the greatest priority (upper right box), followed by phenomena with high importance and medium knowledge (upper center box) and phenomena with medium importance but low knowledge (middle right box). These categories are given a numerical ranking, where Category #1 indicates that highest priority phenomena to investigate (high importance and low knowledge), Category #2 is the next important, etc. Note that each degradation phenomenon was ranked so that a total of seven, equally weighted rankings were used to develop average knowledge and importance levels.

In considering the results of the review, a conservative approach was adopted to determine which phenomena warranted future investigation. Rather than take an average ranking, phenomena were considered based on if any Expert gave it a ranking of 1 (High Importance / Low Knowledge), 2 (High Importance / Medium Knowledge), or 3 (Medium Importance / Low Knowledge). Results from those rankings are given in Figure 8. The excluded phenomena are of such low importance or high knowledge as to not warrant further consideration.

In Figure 8 the open symbols identify phenomena that will be addressed by further investigation while the 'X' symbols show the low ranking of the phenomena that will not be addressed. The degradation concerns that warrant further investigation are grouped into categories with corrosion related phenomena being identified by blue circles, environmentally assisted cracking by green squares, 'other' phenomena by gray triangles and irradiation effects by red diamonds.

The resulting phenomena to be further addressed are presented in Table 11, which summarizes the issues. Note that Table 11 only presents the degradation phenomena for safety-related components. The degradation phenomena are grouped into four categories: corrosion, environmentally assisted cracking,

'other' phenomena, and irradiation effects. For each category, the phenomenon of interest is listed along with a brief description and major variables that additional investigation will address.

Given the materials testing categories in Table 11 (Corrosion, Environmentally Assisted Cracking, Metallurgical Phenomena, and Irradiation Effects), the following sections outline the testing and modelling that will address those concerns. These efforts support appropriate design, operation, and inspection requirements for a [[]] of the structural materials. Unless otherwise noted, all tests will be performed on the base materials (Alloy 316H that meets ASME Section III Division 5 compositional requirements) and on the weld filler metal (ER16-8-2).

4.2 ENVIRONMENTAL COMPATIBILITY

4.2.1 Use of the PIRT Data for NRC Licensing

The PIRT review, which identifies and ranks the appropriate environmental degradation phenomena that are applicable to safety-related components of the KP-FHR (i.e., the reactor vessel which serves the function of retaining the coolant around the fuel).

Note that the environmental testing described below is targeted to satisfy PDC 31 for safety-related components (i.e., the reactor vessel) which operates at approximately 550°C during normal operation and is expected to see higher temperature transients infrequently and for short time periods. To address a large range of potential operational transients as well as many accident scenarios, testing between 600-700°C and environmentally assisted cracking testing between 550-650°C is planned to be conducted. In addition to testing at or above the normal operating temperature of the reactor vessel, many of these tests encompass other aggressive testing conditions such as the use of 'Nominal' Flibe salt rather than redox controlled Flibe or high applied stresses and stress intensity factors relative to what the reactor vessel is expected to see.

Given these conservative test conditions, as well as the extensive testing and analysis plan that was developed from the PIRT process for potential event scenarios higher than the testing conditions, an appropriate statistical analysis of the data from this testing program to extrapolate the results will be used. For example, if corrosion rate at [[]] is of interest, the appropriate prediction interval to bound corrosion rate will be used. An example of an extrapolation of this type is shown in Figure 33, where test data generated at 550°C, 600°C, and 650°C are used to fit a model (solid black line) and a 95% prediction interval (red dashed lines). If these data predicted corrosion rate, for example, then the upper 95% prediction interval would be used to estimate rates at 816°C. Note that additional examples of expected statistical fitting and extrapolation of corrosion data are given in Appendix C.

The PIRT identified two potential accident scenarios that could affect the safety related components, i.e., air ingress and nitrate ingress into the Flibe salt. Note that the KP-FHR technology mitigates these concerns via design features. For example, air ingress is prevented via the hermetically sealed containment and the use of an inert gas overpressure in the reactor vessel. Similarly, nitrate contamination of the Flibe salt is prevented via the design of the intermediate heat exchanger and by operating the Flibe salt at a higher pressure than the nitrate salt. Testing to better assess the effects of air and nitrate contamination of the Flibe salt as detailed below in Section 4.2.3.3 is planned.

A third potential accident scenario, water ingress into the Flibe has been discussed but judged not to be credible for the following reasons. There are two potential sources of water near the reactor vessel, a cavity cooling system, and a decay heat removal system. Both these systems contain design features such that water ingress into the Flibe is not a credible accident scenario as described below.

The potential location of the cavity cooling relative to the reactor vessel is shown schematically below in Figure 25. As shown, cavity cooling is planned to be inside the concrete cavity wall and further separated from the reactor vessel via a steel liner. Given these design features, failures in the cavity cooling do not have a credible path to cause water ingress into the reactor vessel or heat transport system Flibe in any credible operational or event scenario.

Similarly, the decay heat removal concept is based on thermal radiation from the reactor vessel across an air gap to a set of heat removal tubes/panels. The system is physically separated and not in contact with the reactor vessel or Flibe coolant.

4.2.2 Alloys and Heats to be Assessed

Potential heat-to-heat variability in environmental testing was identified in the PIRT. For the known degradation of austenitic stainless steel exposed to fluoride salts, the primary issue is loss of chromium from the grain boundaries to the salt. This grain boundary chromium loss has not exhibited heat-to-heat sensitivity but is fundamentally controlled by the solid-state diffusivity of chromium, a process that is not sensitive to minor changes in alloy composition. For example, recent evaluations show very similar corrosion rates between dual certified 304L/304 stainless steel in Flibe and 316L/316 stainless steel and with a fundamentally based prediction as shown below in Figure 26.

[[

]]

[[

]]

4.2.3 Corrosion

Corrosion tests of prototypic materials to develop quantitative corrosion rate models for Flibe will be conducted. [[

]]

[[

]]

4.2.3.1 Testing Systems

[[

]]

[[

]]

[[

]]

4.2.3.2 The Use of Compositional Analysis and Electrochemical Potential (ECP) Monitoring

Both compositional analysis of the salt and ECP monitoring are planned. [[

]]

[[

]]

[[

]]

[[

]]

[[

]]

[[

]]

[[

]]

[[

]]

[[

]]

4.2.3.3 Corrosion Testing

The planned corrosion testing is summarized in Table 12 which gives the purpose of the test, the materials to be tested, the environment and the approximate test temperatures and duration. For each test, the depth of chromium loss will be assessed over time to establish the governing corrosion kinetics (Equation 1) and to establish the steady state corrosion rate. Note that while the weight change of each corrosion coupon shall be documented, the analytical electron microscopy is intended to be used to determine the extent of corrosion or other metallurgical changes (e.g., Cr loss depth, carbide precipitation, etc.). Additional details of the corrosion testing and an example of the planned statistical analysis of the data are provided in Appendix C.

The purpose of each test is further elaborated in Table 13 and discussed below. For most tests, the corrosion rate will be established by assessing the depth of chromium loss from the sample surface. The chromium loss depth will be determined by an appropriate analytical technique such as wavelength dispersive spectroscopy. In addition, the weight change of the corrosion coupons will be determined. The following bullets expand on the purpose of each test.

$$Cr\ loss\ depth \propto \left(t, \sqrt{t}, \log t, \frac{1}{\log t} \text{ etc.} \right) \quad \text{Eq. 1}$$

- Temperature: The testing as a function of temperature in nominal Flibe for Alloy 316H and ER16-8-2 will determine the corrosion rate for each alloy and will be used as a baseline to judge subsequent separate effects testing. At each of the three planned temperatures, tests will be conducted for different times to determine the controlling kinetics and the steady state corrosion rate. The steady state rates will then be used to develop best-estimate and design-estimate predictions of corrosion rate as a function of temperature. These data will be fit to a model of the form of Equation 2 and provide a standard against which the separate effects tests described below can be quantitatively judged.

$$\text{Corrosion Rate} = A \cdot \sqrt{t} \cdot \text{EXP} \left(-\frac{Q}{RT} \right) \quad \text{Eq. 2}$$

- Microstructural Effects: The effects of the weld heat affected zone, post-weld-heat-treatment, long-term thermal aging, and cold work (20% via rolling) will be assessed and compared to the baseline (temperature dependent models). [[

]]

- Salt Composition: The salt composition testing will assess the effects of the impurities and redox control. The impurity testing will cover accident scenarios defined in the materials PIRT review: nitrate ingress for 168 hours and air ingress for 168 hours (i.e., scenarios 3 and 4). The conditions of the accident scenarios have not been defined at this time and will be provided in safety analysis

reports submitted with a future license application. These tests will determine the effect of potential loss of salt chemistry control on the corrosion rate. Redox control will be investigated via separate effects testing in order to define a factor of improvement in corrosion rate relative to the nominal Flibe purity.

- Occluded Geometry: The intent of these tests is to investigate if a physical crevice influences the corrosion rate with and without redox control of the salt. Occluded geometry will exist on all corrosion samples due to small gaps between samples and the sample cage of RCL systems. The nominal aspect ratio of this crevice is 12 (width/depth) and the minimum aspect ratio is 3.17, based on fabrication tolerances. For a subset of samples, these creviced surfaces will be characterized and compared to fully exposed surfaces. Additionally, unloaded, pre-cracked reference samples used in SCC testing will be used to further evaluate occluded geometry effects. These reference samples will be fitted with an insert which creates long crevices. Note that screening work at ORNL on a nickel-based alloy indicates that crevice corrosion is not a concern in fluoride salt (Reference 87).
- Erosion-Corrosion: These tests will assess the potential effect of erosion-corrosion. Specifically, graphite particulate will be introduced into corrosion tests with flow to assess if hard particles (e.g., potentially from the graphite reflector) will significantly impact corrosion rates. In these tests, weight change of the coupon (via chromium loss depth) will be used as the primary indicator of the corrosion rate.
- Cold Leg Occlusion: In addition to the effect of temperature on the corrosion rate (hot leg samples), many of these tests described above will be used to assess the potential for cold leg occlusion. Cold leg occlusion will be assessed by monitoring the flow rate of salt circulating between hot and cold legs. This rate is estimated using heat flow analysis and furnace power inputs. Additionally, RCL systems will be inspected during planned shutdowns for sample exchanges, and during decommissioning and teardown to look for evidence of cold leg occlusion.

4.2.3.4 CALPHAD Modelling to Inform Corrosion Testing (Information)

Thermochemical tools will be used to help assess the behavior of Alloy 316H and 16-8-2 in molten Flibe. For information, example analyses using these thermochemical methods are shown below. [[

]]

[[

]]

4.2.4 Environmentally Assisted Cracking

Literature data for environmental degradation of both stressed and unstressed samples were recently reviewed in Reference 42. In general, there has been little mechanical testing in molten salts and few data of relevance to the KP-FHR. In part, this is due to the difficulty of conducting in-situ mechanical testing in highly reducing molten salt. An in-situ mechanical testing system was developed to support additional investigation of this phenomena which is shown schematically in Figure 32. Key features of the testing systems include:

[[

]]

The in-situ mechanical testing systems will be used to conduct the slow strain rate, corrosion fatigue, stress corrosion cracking, and in-situ creep testing described below.

4.2.4.1 Slow Strain Rate Testing

Slow strain rate testing (SSRT) will be conducted in nominal Flibe to assess if Alloy 316H, ER16-8-2, and the heat affected zone of Alloy 316H are susceptible to environmentally assisted cracking in fluoride salts. The SSRT is a well-established and accepted methodology to determine susceptibility to stress corrosion initiation and crack growth (Reference 43). Testing will be conducted in accordance with ASTM guidelines outlined in ASTM G129-00 (Reference 44). The SSRT tests will be conducted on flat, pin-loaded specimens. Tests will be conducted at three different temperatures 550, 600, and 650°C, at four (4) strain rates between 1×10^{-6} - 5×10^{-8} (in/in)/sec as detailed in Table 14. In the tests, the degree of an environmental effect will be assessed by comparison of the load/stroke curves with comparable tests conducted in air as shown schematically in Figure 10. Additionally, the fracture mode of these test samples will be investigated to better assess any potential environmental damage.

4.2.4.2 Fracture Mechanics Based Testing: Corrosion Fatigue and Stress Corrosion Cracking

In addition to the slow strain rate testing, fracture mechanics-based testing will be performed on pre-cracked samples based on established methods (Reference 45). These tests will assess prototypical materials (Alloy 316H and ER16-8-2 weld filler metal and the Alloy 316H heat affected zone) and be conducted in nominal Flibe at 550 and 650°C as provided in Table 15. These tests will include both a corrosion fatigue portion of the test and a constant stress intensity factor portion of the test to address stress corrosion cracking. The corrosion fatigue portion of the test will initially be at relatively high ΔK 's to produce fatigue crack growth and will subsequently shed load to both (1) determine the 'Stage II' Paris-law crack growth rate and (2) to prepare the sample for subsequent stress corrosion cracking testing.

These in-salt fatigue crack growth rates will be compared to similar data determined at temperature but in-air to assess any potential degradation, e.g., the difference between in-air vs. in-salt behavior. Example corrosion fatigue data and their comparison to air data are shown in Figure 11. At the completion of the corrosion fatigue portion of the testing, constant stress intensity factor (K_I) testing will be conducted. The intent of these tests is to trigger stress corrosion cracking under aggressive testing conditions and then transition to conditions that are more representative of the KP-FHR. One potential SCC mechanism (strain accelerated corrosion and subsequent intergranular cracking) is shown schematically in Figure 12. Note

that heat affected zone samples will be machined such that the notch of the sample is aligned with the HAZ.

4.2.4.3 Environmental Creep Testing

Creep-rupture testing in Flibe will be conducted to further assess the compatibility of Alloy 316H,ER16-8-2 filler metal, and the Alloy 316H weld heat affected zone with the molten salt. This testing will target creep rupture times on the order of 500 hours and 2000 hours. The creep tests will be conducted at 550°C and 650°C in redox controlled Flibe and will assess the integrated effects of environment and stress on the materials performance. ‘Cross weld’ samples will be used such that the gauge section of the creep sample contains both base metal, heat affected zone and weld metal to best assess a range of materials and microstructures. These creep rupture times will be compared to data from air tests to determine any reduction in creep rupture lifetime due to the salt. Also, the samples will be characterized for chromium loss and compared to unstressed corrosion coupons. The targeted environmental creep test conditions are given in Table 16. Note that replicate tests will only be conducted if significant degradation is observed, e.g., a failure time outside of the 90% confidence interval for air test data and/or if a change in fracture mode is observed.

4.2.5 Metallurgical Effects

The potential environmental degradation phenomena grouped into the ‘other’ category were stress relaxation cracking, phase formation embrittlement, and degradation driven by thermal cycling or by thermal gradients. Each of these phenomena will be addressed to assess the risks of each phenomenon for Alloy 316H. Assessing stress relaxation cracking involves testing in air and as discussed in Section 3.2.2 further analysis and design changes indicate that the risk of this phenomena is sufficiently low such that additional testing is not required.

Testing for phase formation embrittlement addresses the concern that some element could be picked up by the stainless-steel during exposure to Flibe (e.g., carbon or beryllium) and form a deleterious second phase. For example, near-surface carbide precipitation in Alloy 316 exposed to Flibe+ graphite has been noted by Zheng et al. (Reference 18). Similarly, when beryllium metal is coupled to nickel, iron, or stainless steel and exposed to elevated temperature, Be diffuses into the other metal and can exacerbate corrosion rates (Reference 48). When excess Be is present in nickel, iron or similar alloys, Ni-Be precipitates can form and increase corrosion rates, possibly by generating internal stress (Reference 48 and 49). [[

]] These samples will include at least one SSRT sample and one in-situ creep sample as detailed in Table 17.

Lastly, degradation of materials can be driven by thermal phenomena that are influenced by the environment. For example, poor mixing in the coolant could lead to local temperature gradients and result in unwanted thermal stresses (thermal striping). Similarly, the large thermal transients associated with draining and/or filling the reactor vessel could result in ‘ratcheting’ of the pressure vessel. However, several design features and the high Prandtl number of Flibe act to reduce the magnitude of thermal stresses (Reference 50). These phenomena are considered to be appropriately addressed via analysis and specific concerns can be mitigated via design and operational procedures without the need for testing.

4.2.6 Irradiation Effects

The PIRT review identified three irradiation-influenced phenomena that may warrant additional work; irradiation-induced embrittlement, irradiation affected corrosion, and irradiation assisted stress corrosion cracking (IASCC). The following sections describe the additional investigation activities to address irradiation effects. The results of these efforts are to establish the appropriate design, operation, and inspection requirements for the [[]] of the reactor vessel in the KP-FHR. The estimated evolution of dpa and He in the reactor vessel over its lifetime is shown in Figure 13. The high He/dpa ratio stems from the fact that the reactor vessel and core barrel will be shielded by the graphite reflector assembly and hence will be exposed to a thermalized spectrum, leading to boron and nickel transmutation to He. All tests described below will be performed on the base materials (Alloy 316H) and the weld filler metal (ER16-8-2).

4.2.6.1 Irradiation-Induced Embrittlement

The existing published data on austenitic stainless steels indicate that tensile properties at temperatures from 550°C to 650°C are relatively unaffected by < 0.1 dpa and ~10 appm of He when tested at moderate or high strain rates (>10e-3s⁻¹). For example, a compilation of tensile data in Reference 51 indicates virtually no change in yield strength or tensile elongation ≤0.1 dpa for several austenitic stainless steels, including Alloy 316 variants. Similarly, fracture toughness remains high in austenitic stainless steels below 0.1 dpa, with values in excess of 100 MPavm (Reference 52). While most fracture toughness studies focus on LWR conditions (Figure 14), those data indicate that fracture toughness remains high at ~0.1 dpa. Work by Bernard on Alloy 316H (Reference 53) and DeVries on Alloy 304 (Reference 54) at 550°C confirm that fracture toughness is high at conditions of the KP-FHR operation with J_{IC} values near 100 kJ/m². In Figure 14, the apparent increase in toughness at 0.3 dpa may be due to some irradiation-induced hardening before any appreciable loss in ductility, which is reasonable based on the tensile data of Nagae (Reference 51). Based on these literature data, no additional tensile or fracture toughness studies are planned.

However, when testing at low strain rates, stainless steel properties can degrade due to helium embrittlement. An example study of the effect of strain rate and temperature on ductility of an austenitic stainless steel is shown in Figure 15 (Reference 55). As shown in Figure 15, tensile ductility remains unaffected at strain rates ≤ 10⁻² s⁻¹ but slowly degrades as strain rate is lowered, especially in the temperature regime of ~500-700°C. To better assess this effect, literature-reported changes in creep properties after low-dose irradiation in Alloy 316 and Alloy 316 weld metals are summarized in Figure 16. While the data show some scatter, creep strength can decrease by up to ~ 30% after irradiation. Meanwhile, creep ductility is shown to either increase or decrease by up to 20% (in base metal) or 70% (in weld metal) after irradiation.

In order to better define a factor of degradation for creep performance, the effects of irradiation on Alloy 316H and ER16-8-2 will be assessed by post-irradiation testing. The irradiation/post-irradiation testing matrix is shown in Table 18. The target irradiation conditions are designed to be bounding in temperatures (550°C and 650°C), dpa (for example 0.1 and 1 dpa), and He (for example 3 and 15 appm) for the KP-FHR reactor vessel [[]]. Prior to irradiation, the materials will be machined into sub-size specimens typically used for materials-irradiation testing. Post-irradiation creep testing will be performed on the specimens irradiated to 650°C and also tested at 650°C, as summarized in Table 19. Testing at the highest temperature is deemed conservative as creep strength degradation is reported to increase mildly with temperature, as seen in Figure 16 for data point from Aoto, L. et al., (Reference 56) and also reported for

10 dpa-irradiated Alloy 316 (Reference 57). Three stress levels and duplicate specimens will be tested to establish a robust stress/life trend. The results from all post-irradiation creep tests will be compared to unirradiated measurements generated using the exact same specimen geometry and test condition. All specimens will be further characterized via optical and electron microscopy to document any changes in slip and fracture modes.

4.2.6.2 Irradiation-Affected Corrosion

Corrosion in KP-FHR could be affected by irradiation through irradiation-induced changes in the redox potential of Flibe, irradiation-induced changes in the corrosion resistance of stainless steel, or both. In water-based systems, both mechanisms (water radiolysis and defect production in stainless steel) are thought to lead to irradiation-accelerated corrosion (Reference 58). However, these mechanisms are not applicable to the KP-FHR environment. First, Flibe is highly resistant to radiolysis because of the rapid recombination of ions in the molten state. Second, while irradiation could affect the chemistry of Flibe through transmutation, the chemistry control system will have the capability to adjust the redox potential of the salt and correct changes induced by transmutations, expected to be very small. Third, irradiation-induced defect in stainless steel can lead to radiation-enhanced diffusion, which may affect corrosion, but because of the high operating temperature of 550°C and the dpa rate of 0.1 dpa / [[]] the vacancy concentration is not significantly affected by irradiation, and radiation-enhanced diffusion is expected to be minimal.

Existing data indicates that irradiation effects are limited and can be both negative and positive. For example, Lei et al., show a modest increase in post-irradiation bulk corrosion rates (~3X faster) in FLiNaK salt after ~6.18 dpa irradiation with helium ions (Reference 59). In contrast, recent work by Short et al., indicates that simultaneous irradiation and corrosion in FLiNaK acts to minimize intergranular corrosion in molten salt (Reference 60 and 61). Apparently, increased near-surface vacancy concentrations from irradiation accelerates general corrosion (likely controlled via bulk diffusion) but increased intragranular vacancies promotes diffusion from grain interiors to the grain boundary, effectively lowering grain boundary corrosion rates.

Given that: (1) the only safety-related component that is subject to irradiation is the thick-walled reactor vessel, (2) the irradiation dose is quite low < 0.1 dpa and (3) irradiation has shown a benefit to grain boundary corrosion (which is the primary concern), no immediate testing is planned. Instead, irradiation affected corrosion will be assessed via the reliability and integrity management program in the KP-FHR (Appendix B). This plan will utilize surveillance coupons and component monitoring to confirm that the effect of irradiation on corrosion is non-existent or manageable.

4.2.6.3 Irradiation-Assisted Stress Corrosion Cracking (IASCC)

Similar to irradiation affected corrosion, IASCC is not an expected degradation mode in the KP-FHR. The two main pathways for IASCC in water environments are radiation effects on the water chemistry and on the materials (Reference 65). In the KP-FHR environment:

- Radiolysis of Flibe is not a concern, as detailed in in Section 4.2.6.2, and no irradiation-induced changes in the corrosion potential is expected;
- The accumulated dpa in the reactor vessel of <0.1 dpa, which is lower than the lower bound of ~0.3 dpa for IASCC observed in boiling water reactors (Reference 65).

Furthermore, without significant hardening in the alloys at 0.1 dpa (Reference 51), and a potential benefit to grain boundary corrosion rates (Reference 60 and 61), there is no known mechanism by which irradiation would increase susceptibility to IASCC. The testing program will assess if stress corrosion cracking can occur in unirradiated materials (Section 4.2.4). However, available evidence indicates that this is not a credible degradation mechanism under conditions relevant to the KP-FHR. Since this test program is expected to show that there is no direct concern for stress corrosion cracking and since there is no clear means by which irradiation could increase susceptibility (i.e., no expected effect on the coolant chemistry, only a small amount of hardening at 0.1 dpa), no direct IASCC testing is planned at this time. Instead, the KP-FHR reliability and integrity management (RIM) program will assess this area via surveillance coupon and component monitoring as discussed in Appendix B.

5 CONCLUSIONS AND LIMITATIONS

5.1 CONCLUSIONS

Alloy 316H base metal and ER16-8-2 weld filler metal have been selected as the metallic structural alloys for use in safety-significant, high temperature, Flibe wetted component designs. This testing is being conducted to support the design and licensing of both the non-power test reactor (Hermes) and the commercial power generation reactor (KP-X). This testing is focused on structural alloys 316H and ER16-8-2 for the reactor vessel, which was determined to be the only safety significant metallic component of interest, as it serves to retain the Flibe coolant (a fission product barrier) around the fuel pebbles.

The materials testing consists of two major efforts: (1) testing in high temperature air to support ASME design (submitted for information) and (2) testing in molten Flibe salt to account for potential environmental degradation (submitted for review and approval). Testing to support design includes work to extend the code qualification of ER16-8-2 weld metal up to 816°C to match the current qualification of Alloy 316H base metal as well as testing and analyses required to support elastic-plastic and inelastic design per the ASME Code Section III, Division 5.

The environmental effects testing plan detailed in this report is based on an independent Expert Panel PIRT review for the operation of the power generating reactor (KP-X). As detailed in Appendix E, the scope of testing for the non-Power reactor is reduced, based on the lower power and shorter time of operation relative to the power reactor. While not required in the KP-FHR design for structural performance considerations, [[

]]. Appendix A of this report details cladding and coating materials that could be used with safety-related high temperature components of the KP-FHR. Such coatings do not affect structural performance of the underlying base metals and will be used consistent with ASME Section III code requirements.

Kairos Power is requesting Nuclear Regulatory Commission review and approval of the environmental effects testing plan described in this report for metallic structural materials used in safety-related Flibe wetted areas high temperature components of the reactors for use by licensing applicants under 10 CFR 50 or 10 CFR 52. This includes approval of the planned testing and analyses to address potential materials reliability and environmental compatibility issues via design, operation, and inspection. The reactor vessel is credited for maintaining its integrity and retaining fluid to keep the fuel covered in salt during all normal operations and postulated events. The qualification plan for these materials support conformance, in part, to PDC 14 and PDC 31. The qualification plan intends to qualify the reactor vessel and safety-related Flibe wetted areas and to maintain its integrity under the expected environmental conditions of the KP-FHR. The results of the planned tests and analyses, along with a description of the design and inspection program will be provided in a future license application.

5.2 LIMITATIONS

This report is limited to the qualification of metallic structural materials (Alloy 316H and ER16-8-2) for safety-significant, high temperature components in Flibe wetted areas of the KP-FHR.

6 REFERENCES

1. United States Nuclear Regulatory Commission, *Regulatory Guide 1.203, Transient and Accident Analysis Methods*, December 2005. (ML053500170).
2. Barua, B., et al. (2020). *Acceptance Criteria for the Mechanical Integrity of Clad/Base Metal Interface for High Temperature Nuclear Reactor Cladded Components. Pressure Vessels & Piping*. Minneapolis, MN USA, ASME: 1-8.
3. University of California Berkeley Nuclear Engineering. *Fluoride Salt Cooled High Temperature Reactor*. 2015.. [ONLINE] Available at:<http://fhr.nuc.berkeley.edu>. [Accessed 25 June 2020].
4. Kairos Power, LLC, *Design Overview of the Kairos Power Fluoride Salt Cooled, High Temperature Reactor*, KP-TR-001-P, Revision 1. February 2020. (ML20045E423).
5. DELETED.
6. Kairos Power, LLC, *Reactor Coolant for the Kairos Power Fluoride Salt-Cooled High Temperature Reactor*, KP-TR-004-P-A, Revision 1. July 31, 2020. (ML20219A591).
7. Kairos Power, LLC, *Principal Design Criteria for the Kairos Power Fluoride Salt Cooled High Temperature Reactor*, KP-TR-003-NP-A. June 2020. (ML20167A174).
8. Koger, J.W., *Evaluation of Hastelloy N Alloys After Nine Years Exposure to Both a Molten Fluoride Salt and Air at Temperatures from 700 to 560°C*. 1972, Oak Ridge National Laboratory. p. 1-44.
9. McCoy, H. E. and B. McNabb, *PostIrradiation Examination of Materials from the MSRE*, 1972, Oak Ridge National Laboratory. p. 1-104.
10. DeVan, J.H. and R.B. Evans, *Corrosion Behavior of Reactor Materials in Fluoride Salt Mixtures*. 1962, Oak Ridge National Laboratory.
11. Delpech, S., et al., *Molten Fluorides for Nuclear Applications*. Materials Today, 2010. 13(12): p. 34-42.
12. Walters, L., et al., *Sodium Fast Reactor Fuels and Materials: Research Needs*. 2011, Sandia National Laboratory. p. 1-74.
13. Mathew, M.D., R. Sandhya, and K. Laha, *Development of Structural and Steam Generator Materials for Sodium Cooled Fast Reactors*. Energy Procedia, 2011. 7: p. 250-256.
14. Courouau, J.-L., et al., *Corrosion by Liquid Sodium of Materials for Sodium Fast Reactors: the CORRONa Testing Device*, in ICAPP. 2011: Nice, France. p. 1-11.
15. Keiser, J.R., *Status of Tellurium-Hastelly N Studies in Molten Fluoride Salts*. 1977, Oak Ridge National Laboratory. p. 1-31.
16. Keiser, J.R., J.H. DeVan, and E.J. Lawrence, *Compatibility of Molten Salts with with Type 316 Stainless Steel and Lithium*. Journal of Nuclear Materials, 1979. 85&86: p. 295-298.

17. Koger, J.W., *Alloy Compatibility with LiF-BeF₂ Salts Containing ThF₄ and UF₄*. 1972, Oak Ridge National Laboratory. p. 1-52.
18. Zheng, G., et al., *Corrosion of 316 Stainless Steel in High Temperature Molten Li₂BeF₄ (FLiBe) Salt*. Journal of Nuclear Materials, 2015. 461: p. 143-150.
19. McCoy, H. E. and B. McNabb (1972), *Intergranular Cracking of INOR-8 in the MSRE*, Oak Ridge National Laboratory: 1-185.
20. McCoy, H.E., *Status of Materials Development for Molten Salt Reactors*. 1978, Oak Ridge National Laboratory. p. 1-38.
21. Ignatiev, V. and A. Surenkov, *Alloys Compatibility in Molten Fluorides: Kurchatov Institute Related Experience*. Journal of Nuclear Materials, 2013. 441: p. 592-603.
22. Ignatiev, V., et al., *Intergranular Tellurium Cracking of Nickel-Based Alloys in Molten Li, Be, Th, U/F Salt Mixture*. Journal of Nuclear Materials, 2013. 440: p. 243-249.
23. Cheng, H., et al., *Effects of Te on Intergranular Embrittlement of a Ni-16Mo-7Cr Alloy*. Journal of Nuclear Materials, 2015. 461: p. 122-128.
24. Cheng, H., et al., *EPMA and TEM Characterization of Intergranular Tellurium Corrosion of Ni-16Mo-7Cr-4Fe Superalloy*. Corrosion Science, 2015. 97: p. 1-6.
25. McNeese, L.E., *Molten-Salt Reactor Program Semiannual Progress Report*. 1976, Oak Ridge National Laboratory. p. 1-183.
26. vanRooyen, I.J., et al., *Advanced Electron Microscopy and Micro-Analytical Technique Development and Application on Irradiated TRISO-Coating Particles from the AGR-1 Experiment*. 2017, Idaho National Laboratory.
27. *High-Temperature Characteristics of Stainless Steels*, N.D. Institute, Editor., American Iron and Steel Institute: A Designer's Handbook Series. p. 1-44.
28. *The Role of Stainless Steel in Petroleum Refining*, Committee of Stainless Steel Producers. January 1, 1977. p. 1-57.
29. *Material Fabrication and Repair Considerations for Austenitic Alloys Subject to Embrittlement and Cracking in High Temperature 565-760°C (1050-1400°F) Refinery Services*. 2012, American Petrochemical Institute. p. 1-63.
30. Williamson, M., *Pyroprocessing Technologies: Recycling Used Nuclear Fuel for a Sustainable Energy Future*. 2019: Argonne National Laboratory.
31. Choi, E.-Y. and S.M. Jeong, *Electrochemical Processing of Spent Nuclear Fuels: An Overview of Reduction in Pyroprocessing Technology*. Progress in Natural Science: Materials International, 2015. 25: p. 572-582.

32. Simpson, M.F., *Developments of Spent Nuclear Fuel Pyroprocessing Technology at Idaho National Laboratory*. 2012, Idaho National Laboratory. p. 1-23.
33. Sim, J.-H., Y.-S. Kim, and I.-J. Cho, *Corrosion Behavior Induced by LiCl-KCl in Type 304 and 316 Stainless Steel and Copper at Low Temperature* Nuclear Engineering and Technology, 2017. 49: p. 769-775.
34. Kondo, M., et al., *Metallurgical Study on Corrosion of Austenitic Steels in Molten LiF-BeF₂ (Flibe)*. Journal of Nuclear Materials, 2009. 386-388: p. 685-688.
35. DELETED.
36. DELETED.
37. ASME, *Boiler and Pressure Vessel Code*, in *High Temperature Reactors*. 2017, American Society of Mechanical Engineers.
38. International, A., *Standard Test Method for Creep-Fatigue Crack Growth Testing*. 2016, ASTM International. p. 1-19.
39. International, A., *Standard Test Methods for Conducting Creep, Creep-Rupture, and Stress-Rupture Tests of Metallic Materials*. 2018. p. 1-14.
40. ASME, *Development of Weld Strength Reduction Factors and Weld Joint Influence Factors for Service in the Creep Regime and Application to ASME Codes*. 2017, ASME. p. 1-376.
41. Spindler, M., *How to Prevent the Initiation of Cracks in Elevated Temperature Plant - The Gap between Design and Life Assessment*, R. McReynolds, Editor. 2019, EDF Energy. p. 1-34.
42. Young, G.A., M.J. Hackett, and T.-L. Sham, *Materials Challenges for Molten Salt Reactors*, in *1st International Conference on Generation IV and Small Reactors*. 2018, CNS: Ottawa, CA. p. 1-17.
43. Henthorne, M., *The Slow Strain Rate Stress Corrosion Cracking Test - A 50 Year Retrospective*. Corrosion. 72(12): p. 1488-1518.
44. International, A., *Standard Practice for Slow Strain Rate Testing to Evaluate the Susceptibility of Metallic Materials to Environmentally Assisted Cracking*, in *G129-00*. 2000, ASTM.
45. Jones, R.H. and R.E. Ricker, *Mechanisms of Stress-Corrosion Cracking*, in *Stress-Corrosion Cracking*, R.H. Johnes, Editor. 1992, ASM International: Metals Park, OH. p. 1-40.
46. Spindler, M.W. and M.C. Smith, *The Effect of Multiaxial States of Stress on Creep Failure of Type 316H Under Displacement Control*, in *Pressure Vessels and Piping Division Conference*. 2009, ASME: Prague, Czech Republic. p. 1-7.
47. Spindler, M., *Materials Issues in Advanced Gas Cooled Reactors*, R. McReynolds, Editor. 2019: British Energy. p. 1-55.
48. Miller, P.D. and W.K. Boyd, *Corrosion of Beryllium*. 1967, Battelle Memorial Institute: Columbus, OH. p. 1-38.

49. Higgins, J., *Precipitation in the Iron-Beryllium System*. Acta Metallurgica, 1974. 22(2): p. 201-217.
50. Zweibaum, N., et al., *Phenomenology, Methods, and Experimental Program for Fluoride-Salt-Cooled, High-Temperature Reactors (FHRs)*. Progress in Nuclear Energy, 2014. 77: p. 390-405.
51. Nagae, Y., et al., *Irradiation Effect on Mechanical Properties in Structural Materials of Fast Breeder Reactor Plant*. Journal of Nuclear Materials, 2011. 414: p. 205-210.
52. Zinkle, S.J. and G.S. Was, *Materials Challenges in Nuclear Energy*. Acta Materialia, 2013. 61: p. 735-758.
53. Bernard, J. and G. Verzeletti, *Elastic-Plastic Fracture Toughness Characteristics of Irradiated 316H Stainless Steel*, in *Elastic-Plastic Fracture Test Methods: The User's Experience*, ASTM STP 856, E.T. Wessel and F.J. Loss, Editors. 1985, ASTM. p. 131-149.
54. DeVries, M.I. *J-Integral Toughness of Low Fluence Neutron-Irradiated Stainless Steel*. in *13th International Symposium on the Influence of Radiation on Material Properties*. 1987. ASTM.
55. DeVries, M., et al. *Effects of Neutron Irradiation and Fatigue on Ductility of Stainless Steel*. in *Effect of Radiation on Structural Materials*. 1979.
56. Aoto, K., et al., *Effects of Neutron Irradiation on Creep Properties of FBR Grade 316 Stainless Steel*. 1995, International Atomic Energy Agency.
57. Bloom, E.E. and J.O. Stiegler, *On the Microstructure and Creep-Rupture Properties of Type 316 Stainless Steel*, in *STP 529: Effects of Radiation on Substructure and Mechanical Properties of Metals and Alloys*, J. Motef, Editor. 1973, ASTM. p. 360-382.
58. Raiman, S.S., D.M. Bartels, and G.S. Was, *Radiolysis Driven Changes to Oxide Stability During Irradiation-Corrosion of 316L Stainless Steel in High Temperature Water*. Journal of Nuclear Materials, 2017. 493: p. 40-52.
59. Lei, G., et al., *Irradiation Accelerated Fluoride Molten Salt Corrosion of Nickel-Based UNS N10003 Alloy Revealed by X-Ray Absorption Fine Structure*. Corrosion Science, 2020. 165: p. 1-5.
60. Zhou, W., et al., *A Simultaneous Corrosion/Irradiation Facility for Testing Molten Salt-Facing Materials*. Journal of Physics Research B, 2019. 440: p. 54-69.
61. Zhou, W.Y., et al., *Proton Irradiation-Decelerated Intergranular Corrosion of Ni-Cr Alloys in Molten Salt*. Proquest Open Access, 2019: p. 1-11.
62. Cabrillat, M.T., et al., *Intergranular Reheat Cracking in 304H Components. Experiments and Damage Evaluation*, in *SMiRT*. 2001: Washington, DC. p. 1-8.
63. Spindler, M.W., *The Multiaxial Creep Ductility of Austenitic Stainless Steels*. Fatigue and Fracture of Engineering Structures, 2004. 27: p. 273-281.
64. Bradford, R., *Austenitic Reheat Cracking*. 2015. <http://rickbradford.co.uk/T73S04Tutorials.html>.

65. Was, G.S., *Fundamentals of Radiation Materials Science*. 2007, Berlin: Springer-Verlag.
66. Aktaa J., et al., *Effects of hold time and neutron irradiation on the low-cycle fatigue behaviour of type 316-CL and their consideration in a damage model*. 2002. Nucl Eng Des. 213(2–3):111–117. doi:10.1016/S0029-5493(01)00511-8.
67. Pfeil P., et al., *Effects of irradiation in austenitic steels and other high-temperature alloys*. In: *Flow and Fracture of Metals and Alloys in Nuclear Environments*. 1965. ASTM International.
68. Tavassoli A-A., et al., *Data Collection on the Effect of Irradiation on the Mechanical Properties of Austenitic Stainless Steels and Weld Metals*. 1996. Eff Radiat Mater 17th Int Symp.:995-995–15. doi:10.1520/stp16521s.
69. Ward AL., *Thermal and irradiation effects on the tensile and creep rupture properties of weld deposited type 316 stainless steel*. 1974. Nucl Technol. 24(2):201–215. doi:10.13182/NT74-A31475.
70. Messner, M.C., et al., *Finite Element Analysis of Compliant Cladding and Base Metal Systems*. 2018, Argonne National Laboratory.
71. Messner, M.C., et al., *The Mechanical Interaction of Clad and Base Metal for Molten Salt Reactor Structural Components*, in *ASME Pressure Vessels and Piping*. 2018.
72. Barua, B., et al., *Development of Design Method for High Temperature Nuclear Reactor Cladded Components*, in *Pressure Vessels & Piping*. 2020, ASME: Minneapolis, MN, USA. p. 1–8.
73. Barua, B., et al., *Selection Criteria for Clad Materials to Use with a 316H Base Material for High Temperature Nuclear Reactor Cladded Components*, in *Pressure Vessels & Piping*. 2020, ASME: Minneapolis, MN, USA. p. 1–9.
74. Thoma, R.E., *Chemical Aspects of MSRE Operation*. 1971.
75. Not Used.
76. Draemel, D.C., *Faculty Research Associate, UC Berkeley*, G.A. Young, Editor. 2019.
77. Parker, T.D., *Strength of Stainless Steels at Elevated Temperature*, in *Source Book on Materials for Elevated-Temperature Applications*, E.F. Bradley, Editor. 1979.
78. Dhooge, A., *Reheat Cracking - A Reivew of Recent Studies*. International Journal of Pressure Vessels and Piping, 1987.
79. Dhooge, A., *Survey on Reheat Cracking in Austenitic Stainless Steels and Ni Base Alloys*. Welding in the World, 1998.
80. Chabuad-Reytier, M., et al., *Mechanism of Stress Relief Cracking in Titanium Stabilized Austenitic Stainless Steel*. Journal of Nuclear Materials.
81. Soundararajan, S. and T.H. Hamad, *Stress Relaxation Cracking of TP 347H SS Flange Weld Joints on Reactor Charge Heater Manifold in Propane De-Hydrogenation Unit*.

82. Yoon, K.B., J.M. Yu, and T.S. Nguyen, *Stress Relaxation Cracking in 304H Stainless Steel Weld of a Chemical Reactor Serviced at 560°C*. Engineering Failure Analysis, 2015.
83. Chen, B., et al. *Effect of Thermo-Mechanical History on Reheat Cracking in 316H Austenitic Stainless Steel Weldments*. in *Pressure Vessels and Piping*. 2010.
84. Cabrillat, M.T., et al., *Intergranular Reheat Cracking in 304H Components. Experiments and Damage Evaluation*, in *SMiRT*. 2001.
85. Chartrand, P., C. Robelin, and A. Geribi, *A Thermodynamic Model for the LiF-BeF₂-CrF₂-CrF₃-FeF₂-FeF₃-MoF₃-Mo-F₄-NiF₂ System*. 2020, Polytechnique Montreal.
86. Spindler, M., *How to Prevent the Initiation of Cracks in Elevated Temperature Plant - The Gap between Design and Life Assessment*, R. McReynolds, Editor. 2019, EDF Energy.
87. Adamson, G.M., R.S. Crouse, and W.D. Manly, *Interim Report on Corrosion by Alkalai-Metal Fluorides*. 1953, Oak Ridge National Laboratory. p. 1-45.
88. Spindler, M.A., *An Assessment of the Creep Rupture Properties of Type 308 Weld Metal and Type 304/308/304 Weldments Using the PD6605 Procedure*.
89. Spindler, M.W., *The Multiaxial Creep Ductility of Austenitic Stainless Steels*. Fatigue and Fracture of Engineering Structures, 2004.
90. Skelton, R.P., et al., *Factors Affecting Reheat Cracking in the HAZ of Austenitic Steel Weldments*. Pressure Vessels and Piping, 2003.
91. Zweibaum, N., et al., *Phenominology, Methods, and Experimental Program for Fluoride-Salt-Cooled, High-Temperature Reactors (FHRs)*. Progress in Nuclear Energy, 2014.
92. Guo, S., et al., *Corrosion in the Molten Fluoride and Chloride Salts and Materials Development for Nuclear Applications*. Progress in Materials Science, 2018.
93. Kelleher, B., et al., *Observed Redox Potential Range of Li₂BeF₄ Using a Dynamic Reference Electrode*. Nuclear Technology, 2016.
94. Afonichkin, V.K., A.L. Bovet, and V.V. Ignatiev, *Dynamic Reference Electrode for Investigation of Fluoride Melts Containing Beryllium Difluoride*. Journal of Fluorine Chemistry, 2009.
95. Duran-Klie, G., D. Rodrigues, and S. Delpech, *Dynamic Reference Electrode Development of Redox Potential Measurements in Fluoride Molten Salt at High Temperature*. Electrochimica Acta, 2016.
96. Carotti, F., et al., *Electrochemical Sensors for On-Line Redox Measurements in Fluoride Salt-Cooled High Temperature Reactors*, in *American Chemical Society Fall Meeting*. 2020: (Virtual).

Table 1. Summary of Key Parameters for the Power Reactor and the Non-Power Test Reactor

Parameter	Power Reactor	Non-Power Test Reactor
Reactor Description	Low pressure, fluoride-salt cooled, high temperature reactor (FHR)	
Core Configuration	Pebble bed core, graphite reflector, and enriched Flibe molten salt coolant	
Physical Dimensions	Reactor Vessel is ~4 m diameter, ~6 m height	Reactor Vessel is ~2.5 m diameter, ~4 m height
Reactor Thermal Power	320 MW _{th}	up to 50 MW _{th}
Primary Heat Transport System	Flibe Salt, 550°C-650°C, ~0.2 MPa, ~0.11-0.15 m/s	
Intermediate Heat Transport System	Nitrate Salt, < 0.2 MPa, 360°C-600°C	
Power Conversion System	300°C-585°C, steam ~19 MPa	None. Intermediate heat transport system rejects heat from nitrate salt to air
Material for Safety Related Structures	Alloy 316H and ER16-8-2 (ASME Section III, Division 5, approved)	
Lifetime	[[]]	≤ 10 years
End of Life Irradiation of Reactor Vessel	<0.1 dpa	

Table 2. Ranking of Structural Alloys for FHR Applications

	304H	316H	ER16-8-2 Filler Metal	800H	617	Modified Hastelloy N	709	
Code Qualification	●	●	●	●	○	○	○	
Mechanical & Physical Properties	○	●	●	●	●	●	●	
Experience with Molten Salts	○	●	○	●	●	●	●	
Experience in Rx Systems	●	●	○	●	●	●	●	
Technical Maturity	●	●	●	●	●	●	●	
Ability to Procure	●	●	●	●	●	●	●	
Fabrication Considerations	●	●	●	●	●	●	●	
Environmental Compatibility	●	●	●	●	●	●	●	
Regulatory Acceptance	●	●	●	●	●	●	●	
Cost	●	●	●	●	●	●	●	
Summary	Lower strength than Alloy 316H, no compelling advantage			Best combination of properties of current ASME approved alloys. Filler metal matches base properties		High Cobalt undesirable. Ductility decrease with aging		
			Potential application, esp. in nitrate salt. No matching filler metal		Lack of Code Qualification and Supply. No matching filler metal		Desirable for future improvements. 709 filler metal matches properties	
Key	 Little / no work		 Reasonable Work		 Significant work required		 Major work required	
							 Work not initiated, major effort	

Table 3. Summary of Tests to Extend the ASME Qualification of ER16-8-2 to 816°C

[[

]]

Table 4. Summary of Planned Tensile Tests to Support Non-Power Test Reactor Design

[[

]]

Table 5. Summary of Planned Stress Relaxation Tests to Support Non-Power Test Reactor Design

[[

]]

Table 6. Summary of Planned Strain Rate Change (aka ‘stress dip’) Tests to Support Non-Power Test Reactor Design

[[

]]

Table 7. Summary of Uniaxial Creep Tests to Support Non-Power Test Reactor Design

[

]]

Table 8. Summary of Planned Notched Bar Creep Tests to Support Non-Power Test Reactor Design

[[

]]

Table 9. Summary of Planned Creep-Fatigue Tests to Support Non-Power Test Reactor Design

[[

]]

Table 10. Summary of Potential Testing to Assess Stress Relaxation Cracking

[[

]]

Table 11. Summary of Testing and Analysis Judged to be Warranted by the Materials PIRT Review
[[

]]

Table 12. Overall Effects that will be Assessed to Develop Corrosion Rate Models

[[

]]

Table 13. Detailed Plans for Corrosion Testing

[[

]]

Table 14. Summary of Planned Slow Strain Rate Testing to Assess Environmentally Assisted Cracking

[[

]]

Table 15. Planned Conditions for Corrosion Fatigue Crack Growth Rate and Stress Corrosion Cracking Tests

[[

]]

Table 16. Test Conditions to Assess Creep-Rupture Performance in Flibe

[

]]

Table 17. Specimens Planned for Characterization to Assess Metallurgical Effects

[[

]]

Table 18. Target Temperature, Representative Doses, and Estimated Helium Concentrations for Post-Irradiation Tensile and Creep Testing

[[

]]

Table 19. Target Irradiation and Out of Pile Test Conditions for Post-Irradiation Creep Testing

[[

]]

Figure 1. DELETED

Figure 2. Overview of the Commercial Power Generation Reactor Heat Transport Loops with Nominal Operating Temperatures

[[

]]

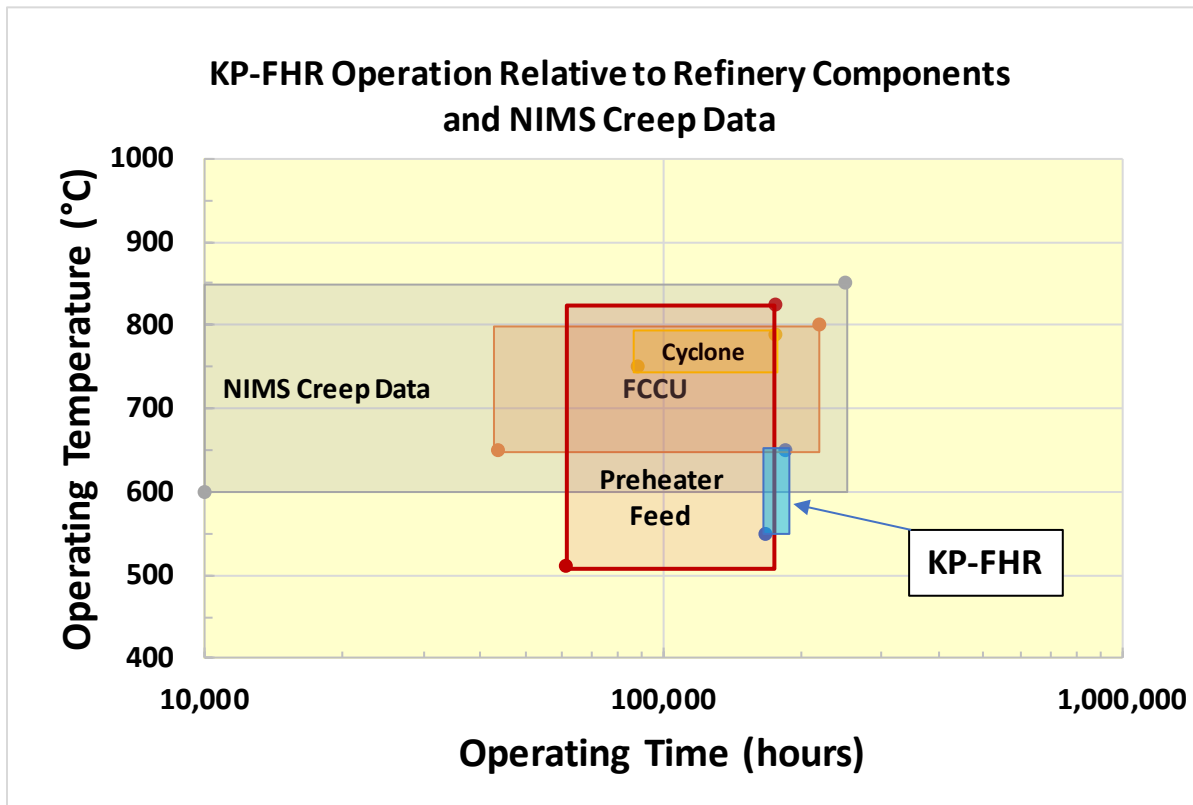
Figure 3. Comparison of the Operating Pressures and Temperatures of Selected Conventional and Advanced Reactor Designs

[[

]]

Note: The labels refer to pressurized water reactors (PWR), boiling water reactors (BWR), high temperature gas reactors (HTGR), and sodium fast reactors (SFR)

Figure 4. Comparison of the Operating Conditions of Alloy 316H in the KP-FHR (blue box) with Oil & Gas Refinery Components and Existing Creep Rupture Data



Note: Application of Alloy 316H and its weld metals in the KP-FHR is consistent with industrial practice

Figure 5. DELETED

Figure 6. Illustration of the Environmental Degradation Mechanisms Considered in the Kairos Power PIRT Review of Environmental Degradation

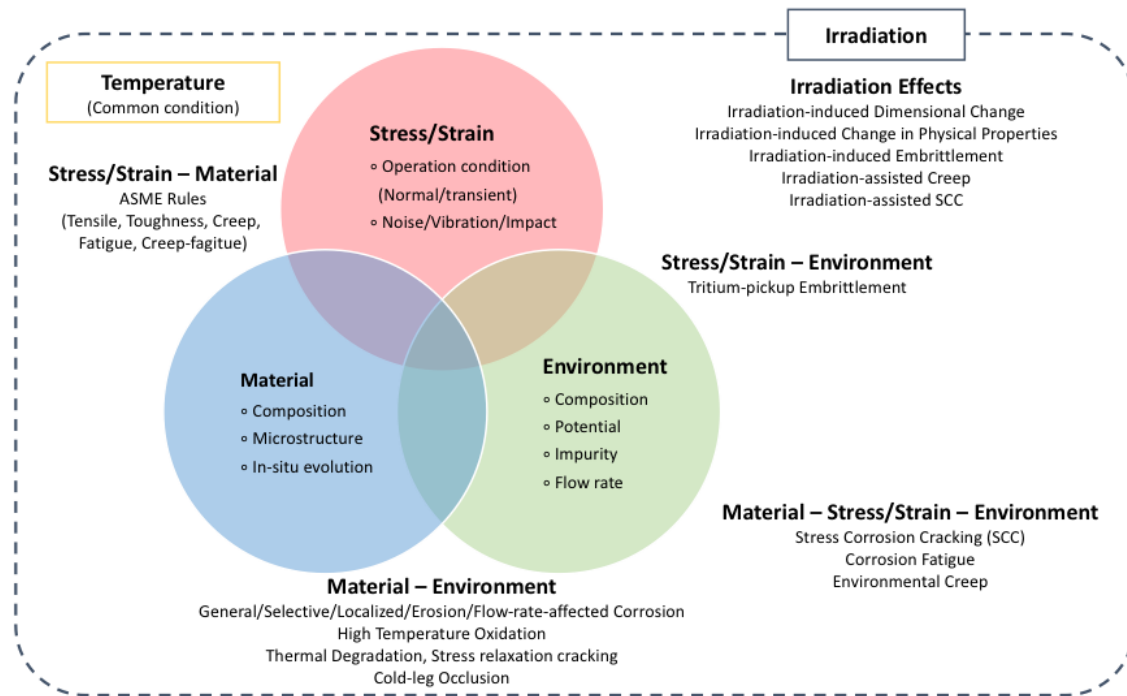


Figure 7. The Knowledge and Importance Rankings Used by the Expert Panel to Assess Environmental Degradation Phenomena

		Knowledge		
		High	Medium	Low
Importance	High	Category #4	Category #2	Category #1 (most important)
	Medium	Category #6	Category #5	Category #3
	Low	Category #9 (least important)	Category #8	Category #7

Figure 8. Summary of the PIRT Rankings

[[

]]

Figure 9. DELETED

Figure 10. Illustration of Slow Strain Rate Testing (SSRT) Data (left) and How the Results May Be Used to Map Out Regimes of Susceptibility to Environmentally Assisted Cracking (right)

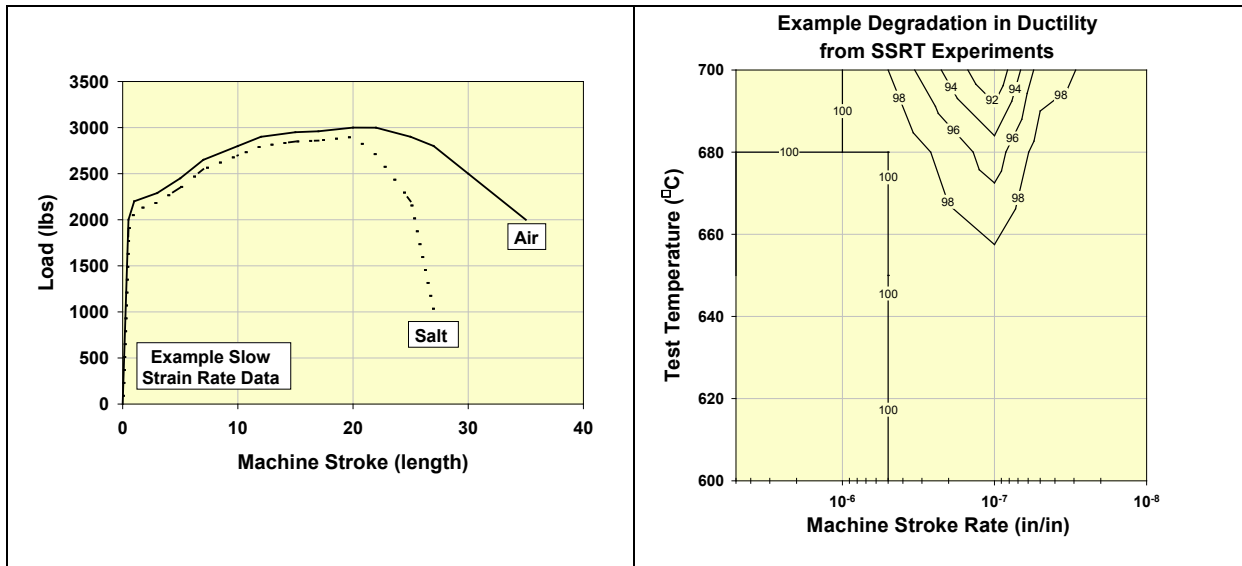


Figure 11. Example Corrosion Fatigue Crack Growth Rate Data (left) and How They Will be Compared to Data Collected in Air (right) to Assess the Effect of Environment

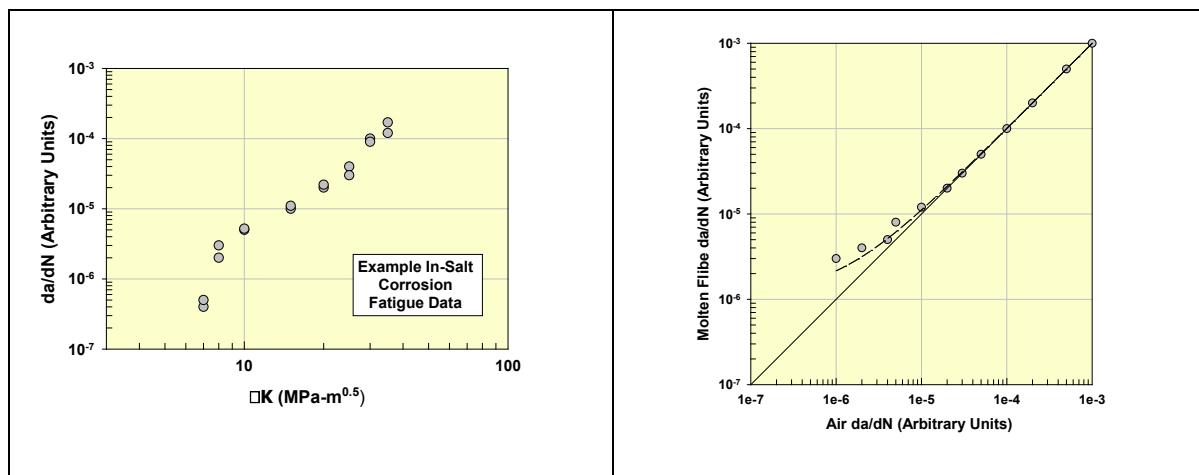


Figure 12. Illustration of a Potential SCC Mechanism in Flibe (top) where Grain Boundary Cr Loss is Accelerated at a Strained Crack Tip and (bottom) Schematic SCC Growth Rate Data

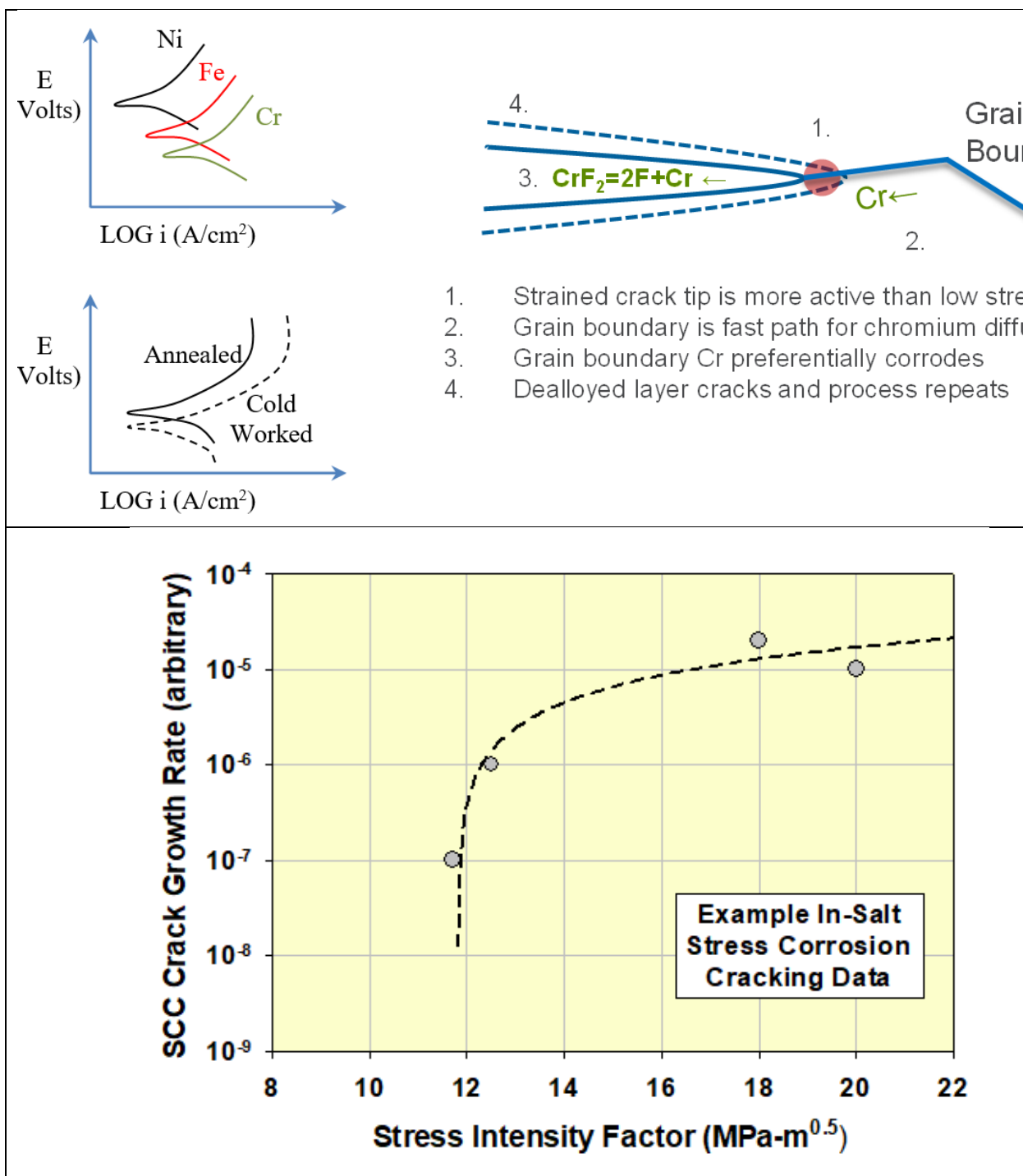


Figure 13. Comparison of the Evolution of Irradiation Damage and Helium Generation in the KP-FHR Reactor Vessel

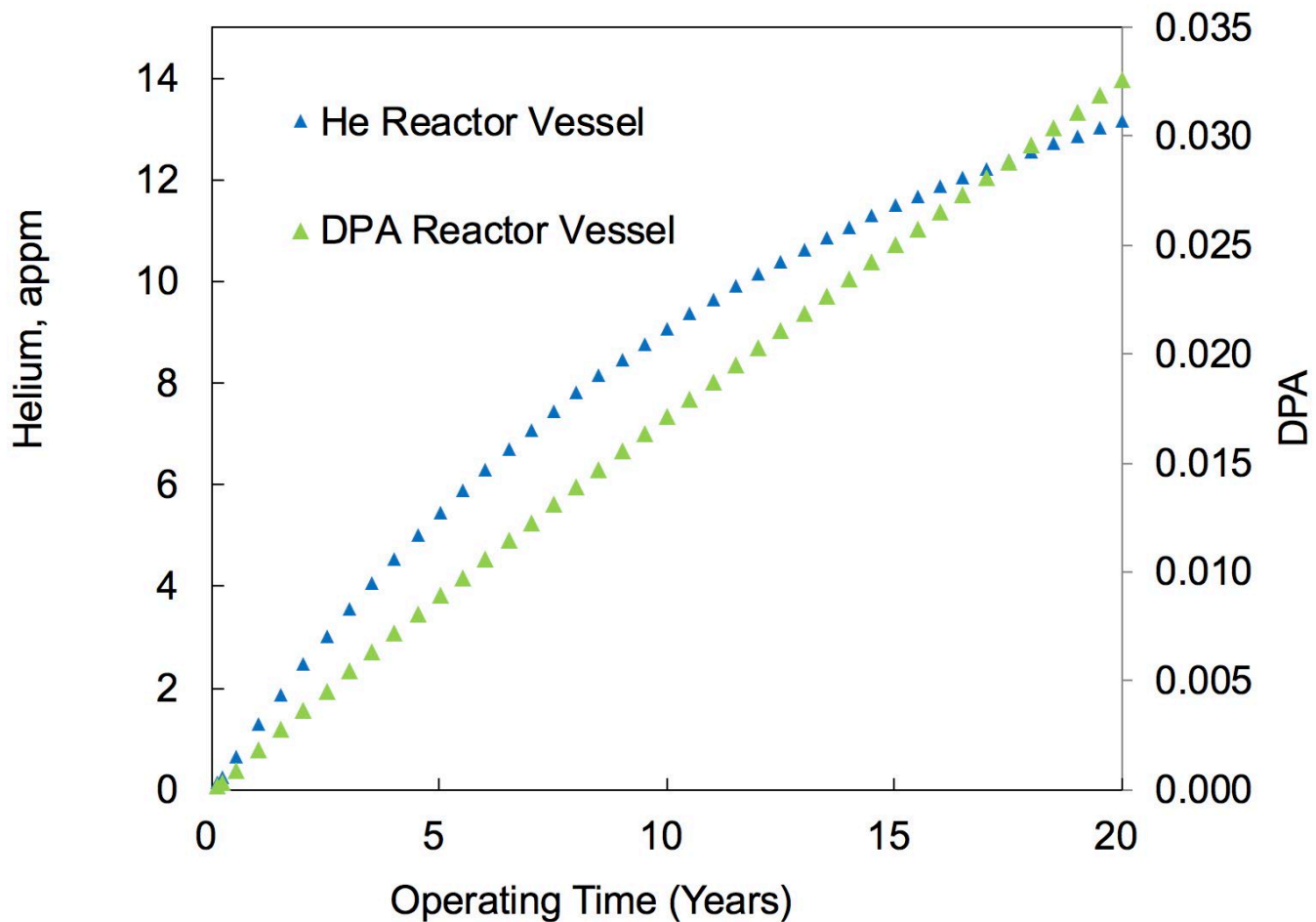
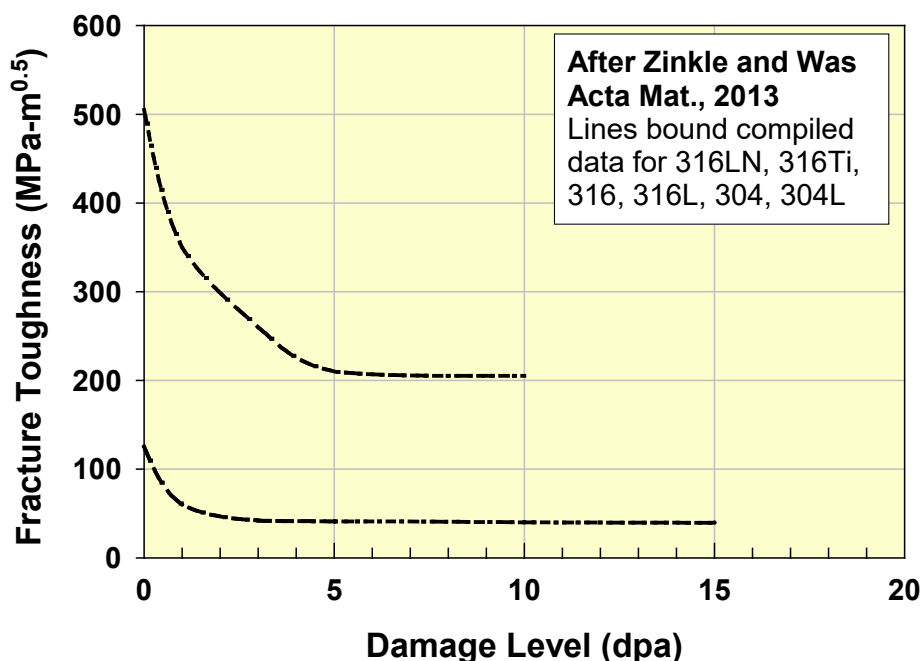
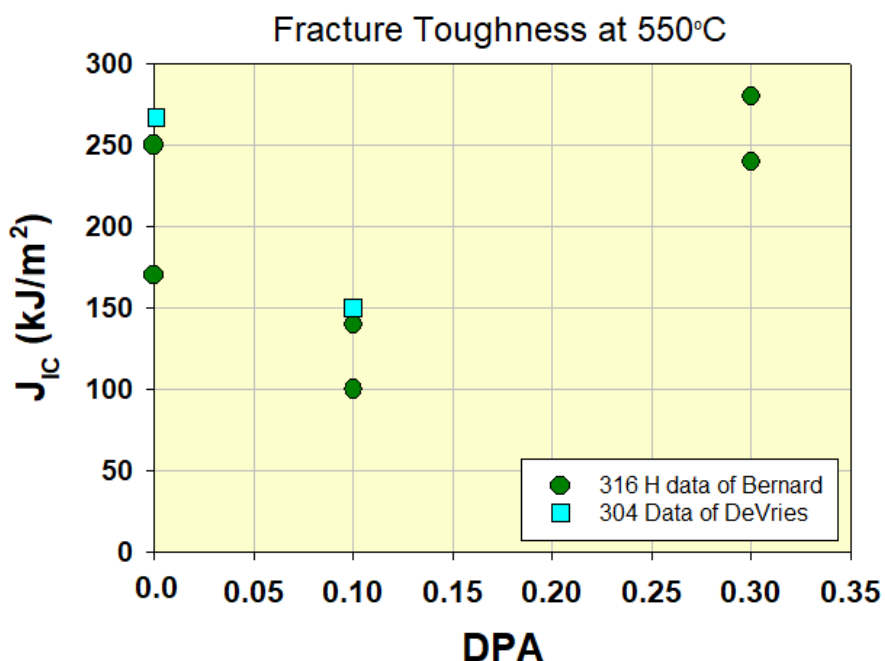


Figure 14. How Irradiation Affects Fracture Toughness in Austenitic Stainless Steels and Specific Data for Alloy 316 and 304 at 550°C.



Note: Reference 52



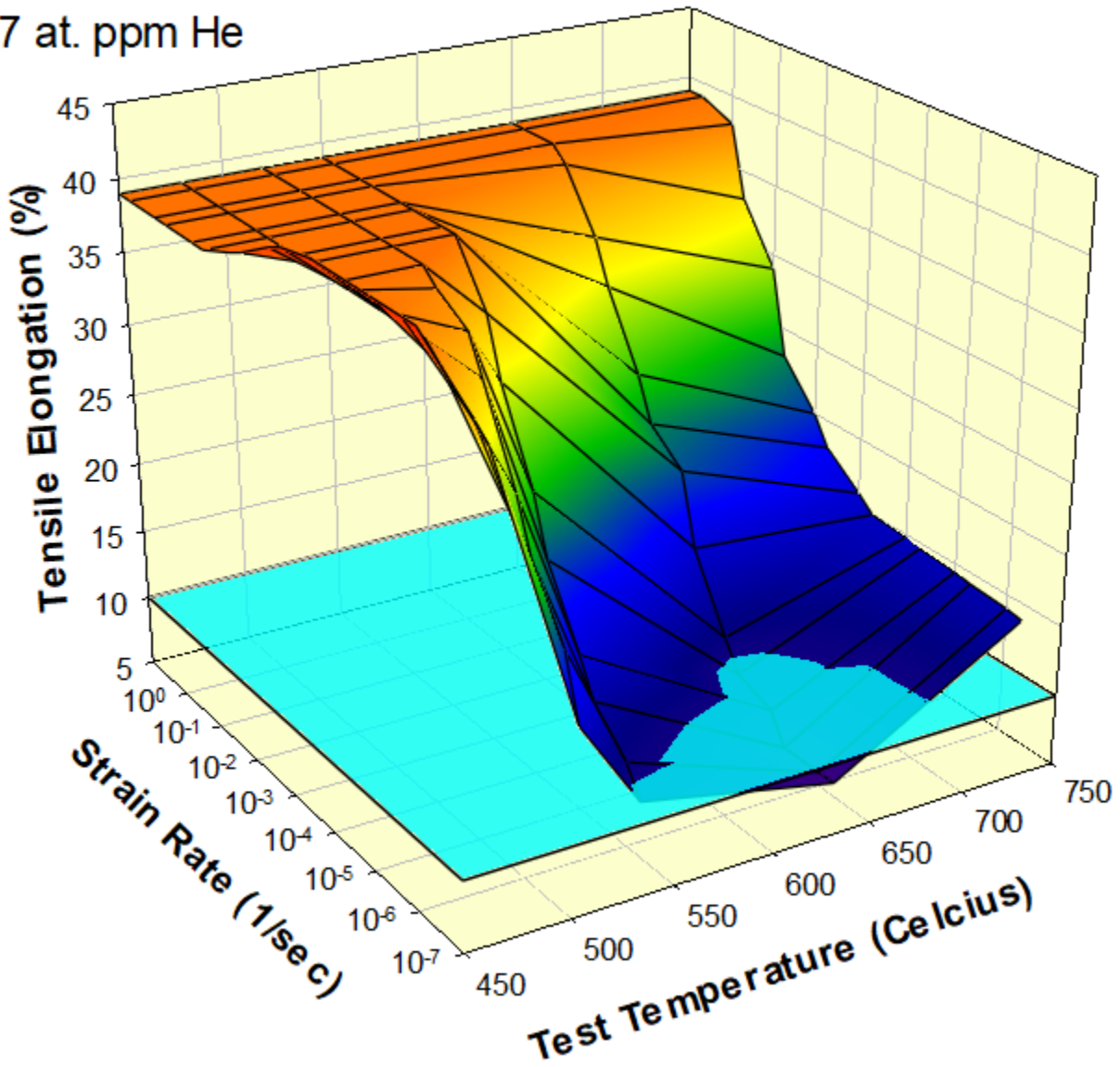
Note: Reference 53 and 54

Figure 15. Illustration of How Strain Rate and Temperature Affect Tensile Ductility in an Austenitic Stainless Steel Irradiated to a Helium Content of ~7 at. ppm

Data of De Vries 1979

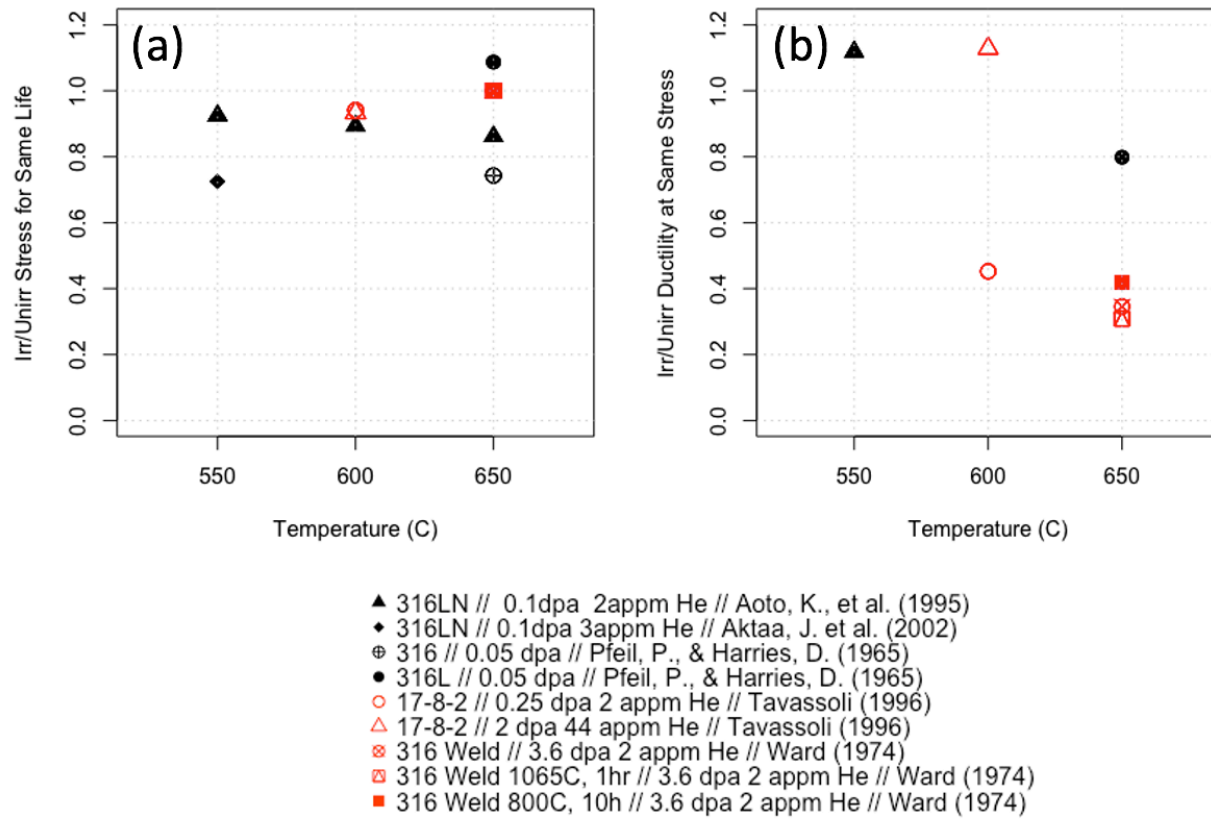
Thermal Fluence: $2 \times 10^{24} \text{ n/m}^2$

7 at. ppm He



Note: Reference 55

Figure 16. (a) Normalized Creep Strength After Irradiation (Ratio of Irradiated Stress to Unirradiated stress to Reach the Same Average Creep Life) (b) Normalized Creep Ductility After Irradiation (Ratio of Irradiated Ductility to Unirradiated Ductility at the Same Stress)



Note: References 56, 66, 67, 68, 69

Figure 17. Variable Corrosion Rate of Alloy 316 Stainless Steel with Time (top) and The Strong Benefit of Be Addition (Redox Control) (bottom).

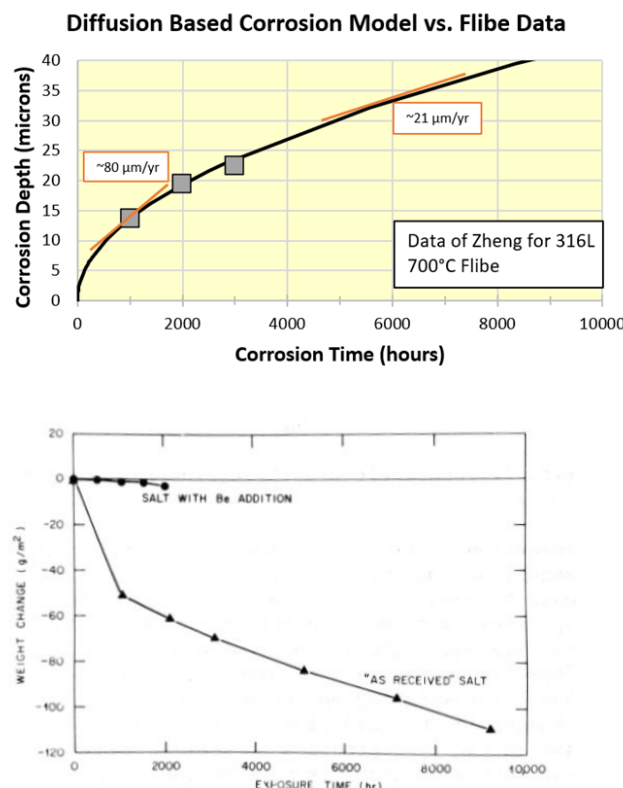
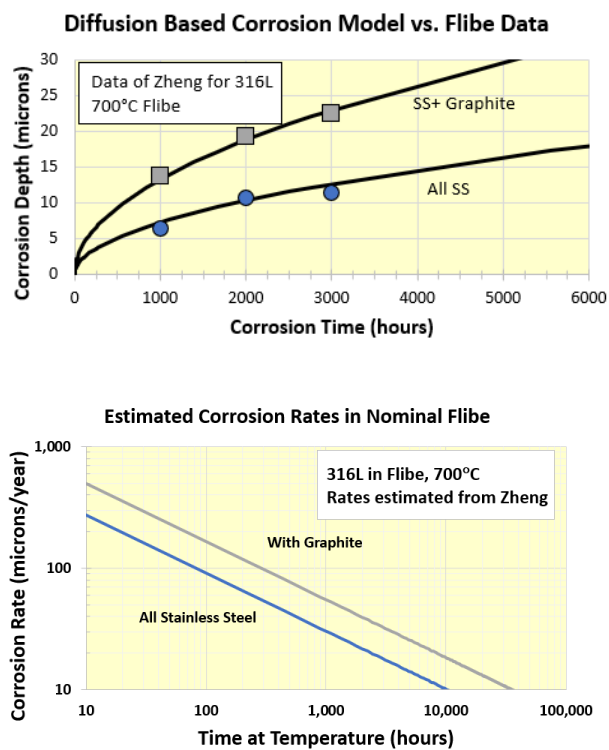


Fig. 2. Weight change versus exposure time for type 316 stainless steel in LiF-BeF₂ salt at the maximum loop temperature of 650°C.

Figure 18. Data of Zheng et al, Illustrating the Effect of Graphite on the Corrosion Depth (top) and Corrosion Rate of Alloy 316L in Flibe at 700°C (right)



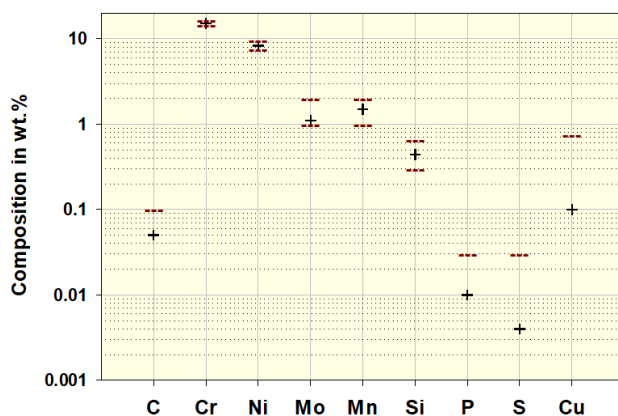
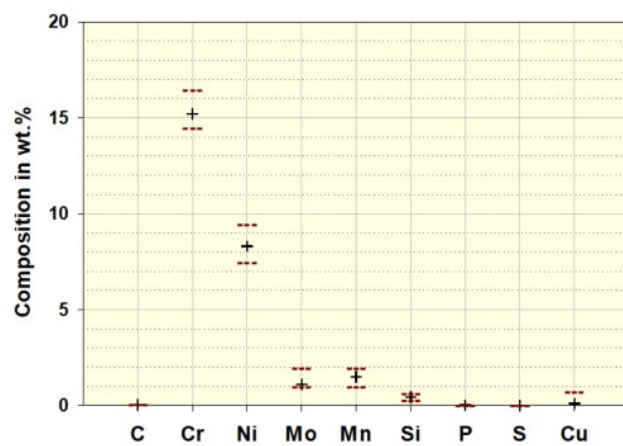
Note: The difference in corrosion rate is just less than 2X

Figure 19. Examples of Weld Pad Buildups (top) and A V-Groove Weld (bottom) used to Fabricate Test Samples

[[

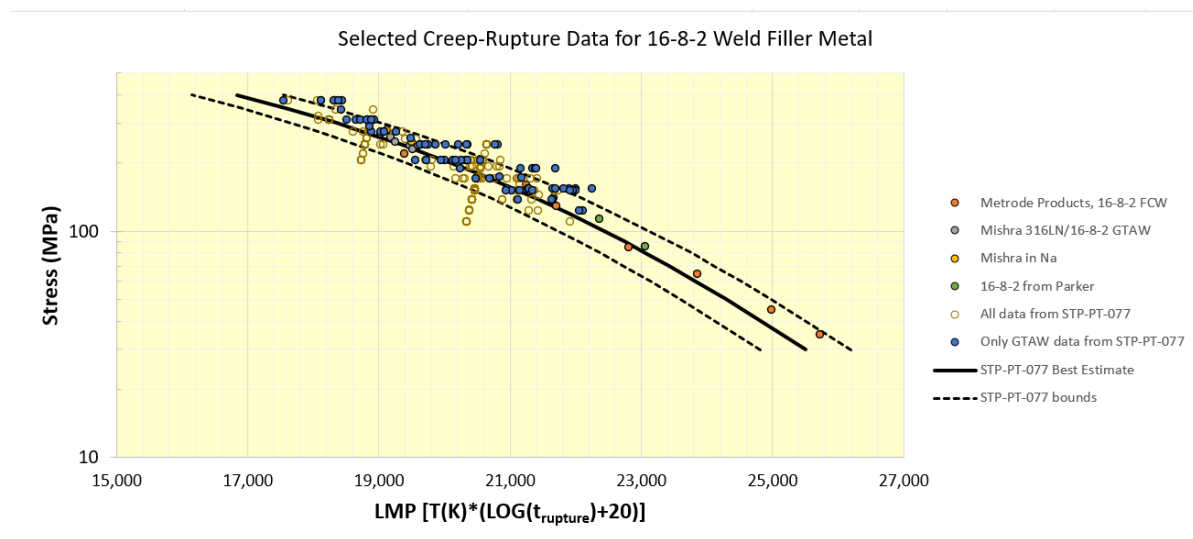
]]

Figure 20. Comparison of the Composition of Heat 578409 (+ symbols) Relative to the ASME Code Specification (dashed lines, from Section II. 2017)



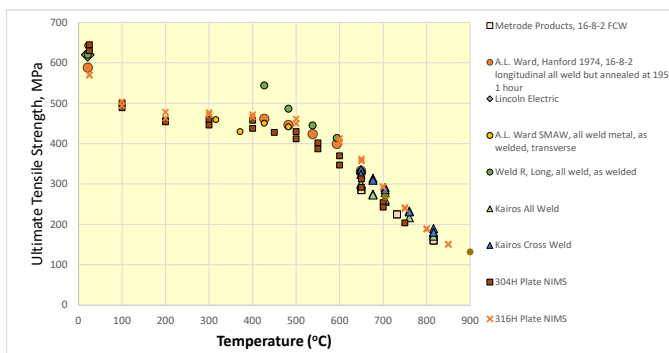
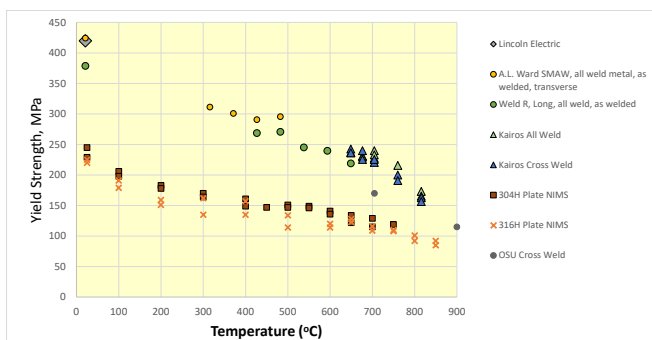
Note: C, P, S, and Cu only have maximum specifications. Linear scale (top) and log scale (bottom) to better illustrate the elements at low concentrations.

Figure 21. Selected Creep-Rupture Data for ER16-8-2 Weld Filler Metal Compared to the Best Estimate Prediction and Confidence Bounds



Note: Presented in STP-PT-077. The ASME Code Case data will be assessed relative to relevant data and appropriate statistic bounds determined.

Figure 22. Comparison of Selected Base Metal and Weld Metal Tensile Data



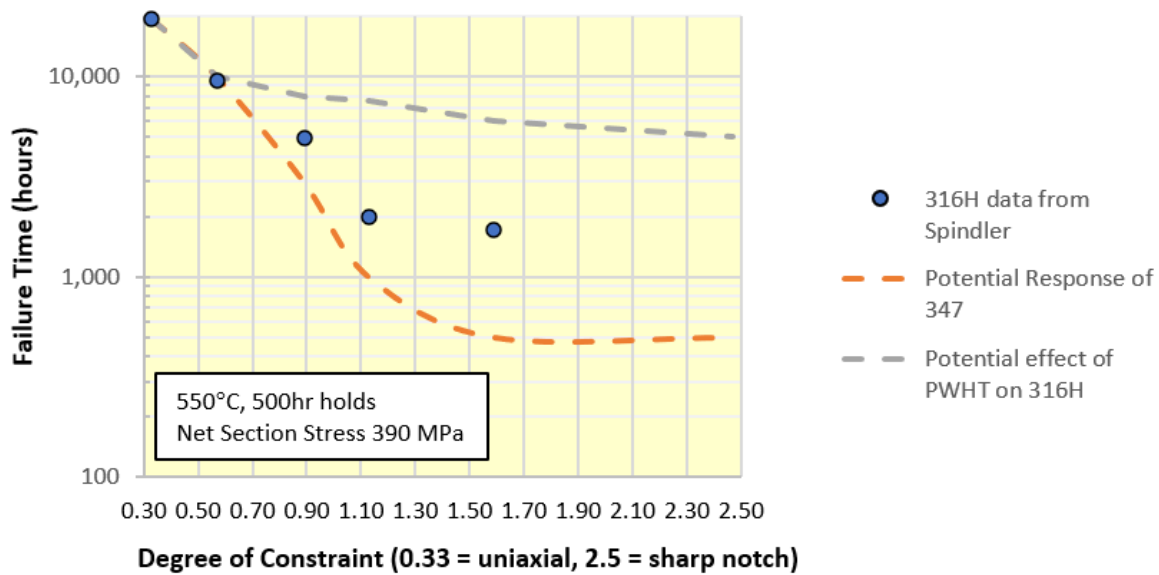
Note: Yield strength shown on the top and ultimate tensile strength on the bottom.

Figure 23. Weld Designs that Minimizes the Risk of Stress Relaxation Cracking

[[

]]

Figure 24. Notch Bar Testing Used to Assess the Susceptibility of Alloy 316H Stainless Steel to Stress Relaxation Cracking



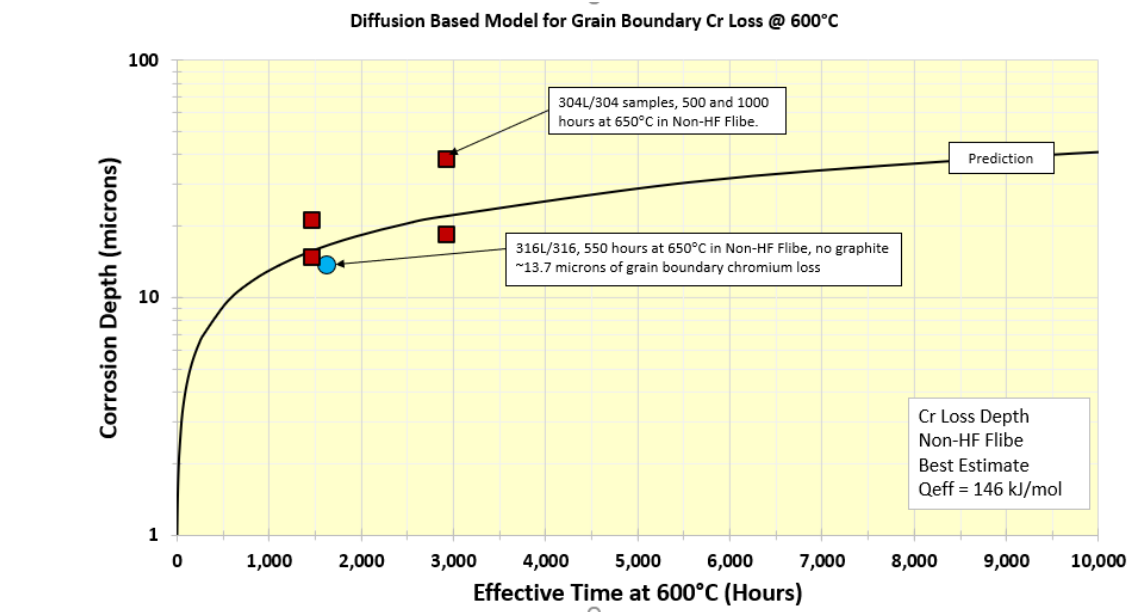
Note: Relative to other Alloys assesses the effects of metallurgical variables such as post weld heat treatment.

Figure 25. Potential Location of the CCS Relative to the Reactor Vessel

[[

]]

Figure 26. Predicted Grain Boundary Diffusion Rate



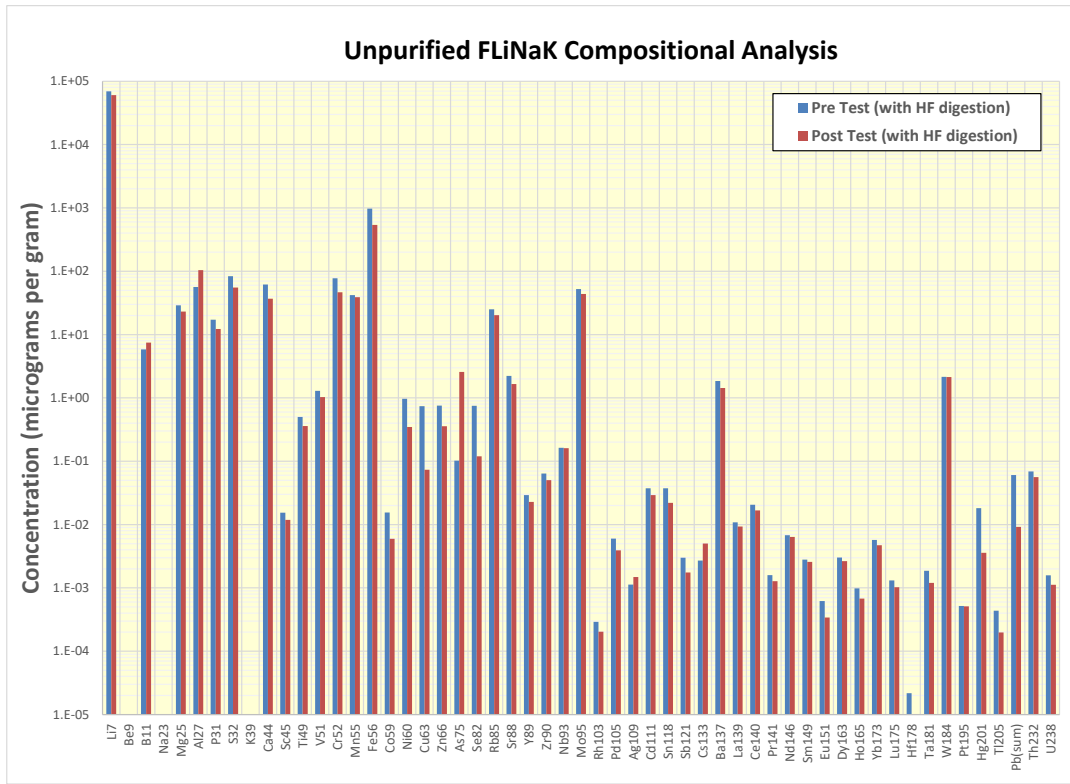
Note: Predicted grain boundary diffusion rate (solid black line) with recent data for Alloy 304 (red points) and Alloy 316 (blue point). The similar rates between the Alloys 316L/316 and Alloys 304L/304 (within 2X) support the notion that heat-to-heat variability will be minimal.

Figure 27. Schematic Illustration of a Rotating Cage Loop (RCL) Corrosion Testing System (left) and an Operational RCL System (right)

[[

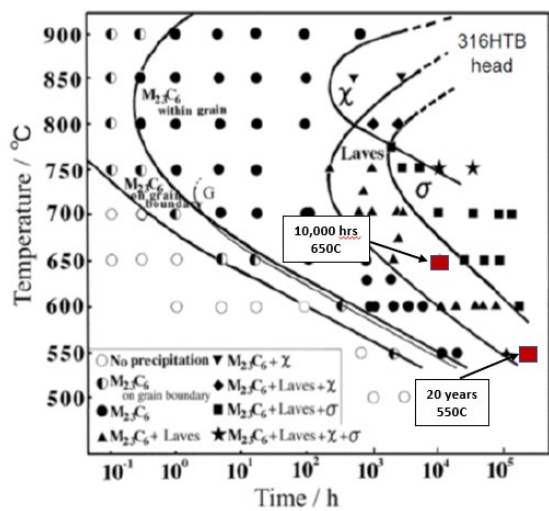
]]

Figure 28. Example of Fluoride Salt Compositional Analysis



Note: Unpurified FLiNaK before and after SSRT testing a Alloy 316L sample at 600°C and 1e-6 (in/in)/sec

Figure 29. The Time-Temperature-Transformation Diagram for Alloy 316H



Note: Targeting 700°C for 10,000 hours as an aging treatment to represent long time operation at 550°C
(Reference 82)

Figure 30. Calculated LiF-BeF₂ Phase Diagram Against Experimental Data

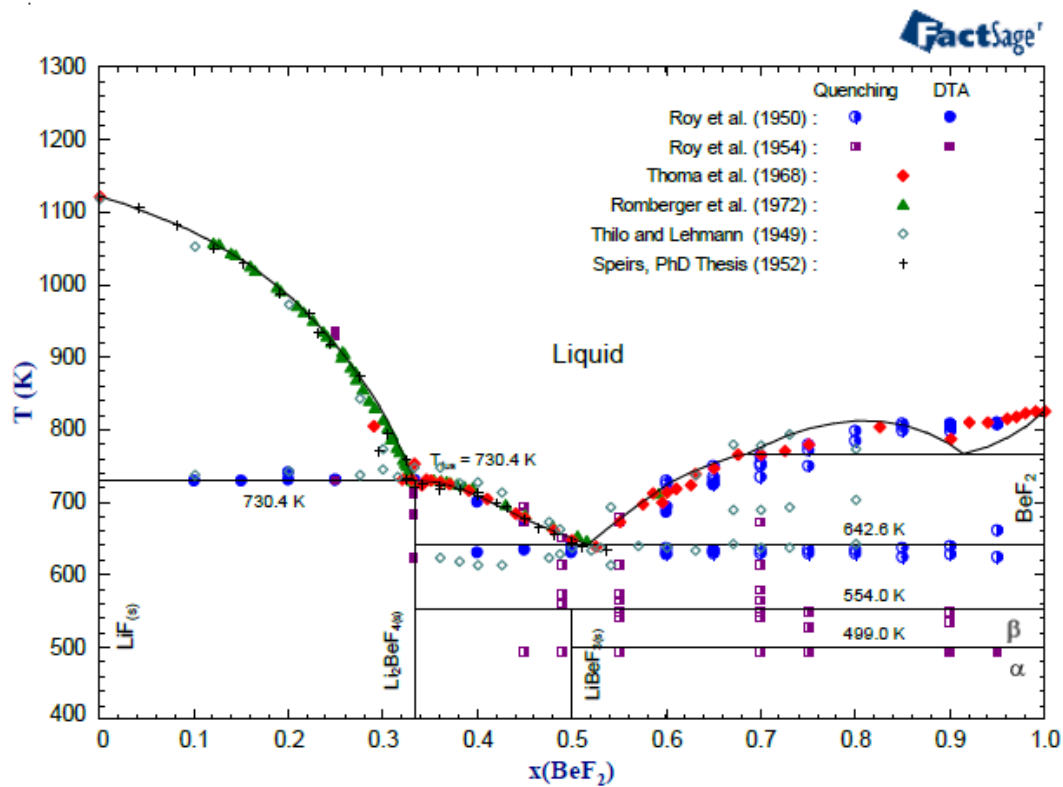
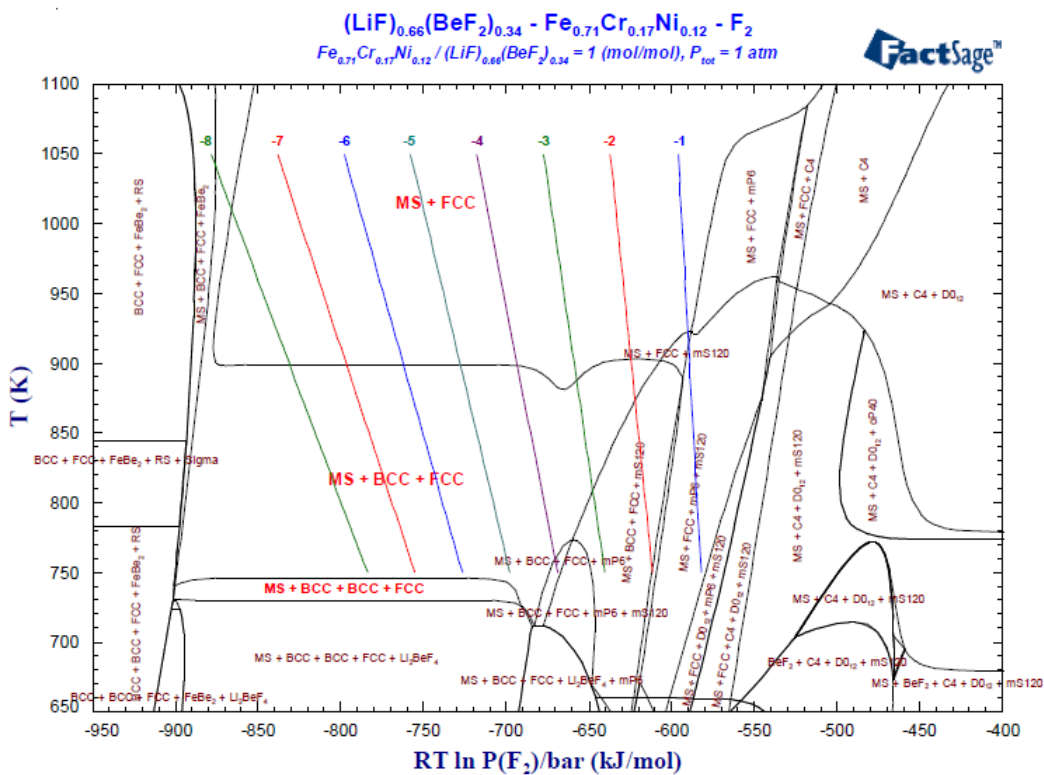


Figure VI-1 : Calculated LiF-BeF₂ phase diagram.

Figure 31. Calculated Multicomponent Phase Diagram with Superimposed Log (p(HF))



Note: The diagram shows regions of metal stability as well as the concern of FeBe_2 formation if conditions are overly reducing.

Figure 32. Schematic of the In-Situ Mechanical (ISM) Testing Systems (left) and an Operational ISM Running a Slow Strain Rate Test in FLiNaK Salt (right)

[[

]]

Figure 33. Example Fitting and Extrapolation of Degradation Rate

[[

]]

APPENDIX A. COATINGS, CLADDING, AND TRITIUM MANAGEMENT

The design of the KP-FHR does not require the use of cladding or coatings. However, these materials may be desirable to optimize the performance of the reactor system. [[

]] Some cladding and coatings materials of interest are listed in Appendix A, Table 1, for information.

Cladding and Coatings for Salt Facing Applications

Current ASME Section III Division 5 Code rules for cladded structural components in elevated temperature service are limited. ASME Section III Division 5, Paragraph HBB-2121 allows non-Code qualified materials to be used for cladding if the clad thickness is 10% or less of the thickness of the base material. ASME Section III Division 5, Paragraph HBB-3227.8 specifies that no structural strength will be attributed to the cladding in satisfying the primary load stress limits. It also requires that the cladding will be considered in design evaluation related to limits on deformation-controlled quantities, i.e., strain accumulations due to ratcheting and creep-fatigue damage but does not provide guidance or requirements for that assessment. While the 10% clad thickness rule allows Kairos Power to select corrosion-resistant materials that are not Code qualified for Class A service, the lack of design rules presents challenges in their application.

In order to help enable the application of corrosion-resistant coatings and cladding, Kairos Power is working with Argonne National Laboratory as part of a GAIN research collaboration (References 70, 71, 72, and 73) (Gain cladding project under contract No. DE-AC02-06CH11357 with the US Department of Energy). The GAIN research includes establishing the mechanical nature of the cladding or coating (compliant or elastic), determining key mechanical properties (yield strength, creep rate), assessing the integrity of the coating after thermal cycling, and testing the environmental compatibility of the cladding or coating in molten Flibe salt. While this program is under development, it is expected to result in the ability to use cladding and coatings with ASME Section III Division 5 structural materials.

Coatings and claddings used in the KP-FHR to decrease tritium permeability will mainly be applied to salt facing surfaces because the benefit of a tritium permeation barrier is expected to increase for salt facing applications compared to the air side. Since the tritium permeation barrier coatings and claddings will be exposed to molten Flibe, the corrosion resistance of barrier materials will be evaluated, and the selection of tritium permeation barrier materials will be limited to those which provide comparable or improved corrosion rates in Flibe compared to Alloy 316H. In addition to Flibe facing tritium permeation barriers, the KP-FHR design may also include nitrate salt-facing coatings which would assist in reducing the permeation of tritium through the intermediate loop piping.

[[

]]

Cladding and Coatings for Air Side Applications

For the application of cladding or coatings on the air side of safety-related systems, there are no ASME design rules governing their use. Potential applications for coatings on the air side of these systems include oxide films [] surface treatments to enhance thermal emissivity or providing anti-galling. If coatings are used on the air side of safety-related systems, the benefit of the treatment will be demonstrated and confirmed through analysis and/or testing that there is no significant degradation to the underlying structural material.

Appendix A Table 1. Comparison of Selected Coatings and Cladding of Interest to the KP-FHR

[[

]]

APPENDIX B. INSPECTION AND AGING MANAGEMENT

Introduction

Nuclear Power Plant component life management requires a combination of analysis, inspection, testing, and monitoring activities. The information derived from each of these activities complements one another and should be utilized as part of an integrated program. Qualification through mechanical and environmental testing is the first step in ensuring material performance for long-term service in nuclear power plants. While test plans can to some extent account for combinations of mechanical and environmental factors that affect material performance, it is rare that laboratory testing can account for all of the variables and interactions present during reactor operation. Furthermore, it is often impractical to perform laboratory tests for times on the order of the expected component lifetimes (usually decades). While the material qualification test programs described in this document provide confidence that Alloy 316H / ER16-8-2 will perform satisfactorily over the service life of the plant; in-service monitoring and evaluation throughout the plant life will be used to further ensure the safe and reliable operation of the KP-FHR.

Reliability and Integrity Management (RIM)

ASME Section XI has historically provided rules for in-service inspection and the replacement and repair of components during the operating life of light water reactors. The unique physical features of high temperature reactors such as the KP-FHR present a new paradigm for RIM that has required the Code to develop new approaches. The new approach being implemented as ASME Section XI Division 2 "Reliability", applies to any type of reactor design, and was published for the first time in the 2019 Edition of the ASME code.

The new RIM allows a combination of Monitoring and Non-Destructive Examination (MANDE) methods for an aging management program. The ability to use both monitoring and non-destructive examination is a significant advantage to many advanced reactor designs, including the KP-FHR, since their compact size and need for coolant chemistry control limits access to some components during the operating lifetime of the plant. While the 2019 Edition of ASME Section XI Division 2 outlines the top-level requirements for a RIM program, Mandatory Appendix VII of Division 2 will describe the specific MANDE methods and acceptance criteria for each of the different types of advanced reactors. Note that Article VII-4 has been reserved for Molten Salt Reactors (and presumably FHR designs) but has not yet been developed in detail. Kairos Power is active with the Section XI Committee Sub-Groups and Working-Groups related to RIM and MANDE and plans to apply the KP-FHR experience to the development of relevant Code articles for FHRs.

Development of the RIM program for the Kairos Power plant will be performed in accordance with the requirements of ASME Section XI 2019 Edition, Mandatory Appendix I ("RIM Decision flowcharts for use with the RIM") and Appendix II ("Derivation of component reliability targets from plant safety requirements"). Component Level Reliability Requirements will be derived from Plant Level Reliability Requirements through the Probabilistic Risk Assessment process. With Reliability Targets established, components will be assessed for mechanisms of environmental degradation and modes of failure as derived from the Phenomenon Identification and Ranking Table. Critical flaw size will be determined for the most likely modes of failure in each component. Monitoring and Non-Destructive Examination technologies will be evaluated for the capability to detect sub-critical flaws and to endure the relevant inspection environments. Technologies and inspection schedules will then be selected for each area of

interest to ensure that flaws can be detected before they grow to critical flaw size. Material performance will be monitored during operation, and data will be fed back to update the MANDE schedule throughout the life of the plant. The specific details of a RIM program for the KP-FHR will not be available in the near-term but will be provided with the Operating License application.

Surveillance Coupons

In-situ surveillance specimen programs have played an important role in materials degradation management in the Light Water Reactor industry since the 1970's and a similar program will be needed to validate our understanding of long-term material performance in the KP-FHR environment. In Light Water Reactors, one focus of the surveillance specimen program has been to monitor the degradation of fracture toughness of low-alloy steel reactor vessel materials with irradiation. Similarly, the surveillance specimen program for the KP-FHR will provide insight into the long-term combined effects of exposure to Flibe salt, irradiation, and high temperatures. A series of specimens will be strategically placed throughout the reactor vessel to provide coupons with a range of temperature and radiation exposure. These samples will be monitored throughout the life of the plant and assessed for changes in composition, phase stability, microstructure, and mechanical properties. These coupons will also be used to assess irradiation-affected corrosion, and irradiation-assisted stress corrosion cracking. The specific surveillance coupon program will be provided at the time of the Operating License application.

APPENDIX C. DETAILS OF THE CORROSION DATA ANALYSIS

Many testing programs that are expected to yield quantitative results were developed with the intent of statistical analysis of the data. For example, the general corrosion testing of Alloy 316H and ER16-8-2 plans include three samples per condition, conducted over a wide range of times and temperatures. These data will be analyzed via electron microscopy of corrosion coupon cross sections which, we believe, is superior and more sensitive a measure than weight change.

With those corrosion data, Kairos Power will develop ‘baseline’ corrosion models for Alloy 316H and ER16-8-2 and conduct separate effects tests to assess key variables that include microstructure, contaminants, redox control, occluded geometry, and erosion-corrosion. Statistical analysis such as Analysis of Variance (ANOVA) will be used to establish the significance of these variables on the response model of corrosion rate compared to random error. Furthermore, the corrosion model will utilize appropriate prediction bands to ensure appropriate and conservative extrapolation from test conditions to KP-FHR operational times and temperatures.

Note that some testing may not be amenable to statistical analysis but is being performed to develop understanding and guidance. For example, the slow strain rate tests in Flibe are being performed primarily to assess regimes in which environmentally assisted cracking may occur. In these tests, a change in response (load vs. stroke) relative to air testing and post-test analysis of the fracture path will be used to develop understanding of the degree of concern for cracking. Similarly, stress corrosion cracking tests are being conducted to better understand if this phenomenon occurs in environments and mechanical conditions of relevance to the KP-FHR. Depending on the response of Alloy 316H and ER16-8-2 to these tests, a statistical analysis of the data may be used but also may employ fundamental materials science and engineering judgement to develop appropriate design factors or other practices (e.g. periodic inspection) that will appropriately address the concern of environmentally assisted cracking.

Note that corrosion rates can be confounded by complicating factors such as carbon pickup during testing as well as the difficulty in removing dried salt from test coupons. To mitigate these factors, Kairos Power will use electron microscopy of corrosion coupon cross sections as the primary method to assess corrosion (e.g. depth of chromium loss) as well as other compositional changes (e.g. the extent of Fe and Ni loss, the precipitation of Mo-rich Laves phase, and the precipitation of carbon rich phases). An example of this analysis is given below in Appendix C, Figure 1.

For information, an example of expected statistical analysis of corrosion data is presented below. In this example, the corrosion data of Zheng et al. (pink squares) are used to generate example corrosion data for three different temperatures and for times up to 10,000 hours (Reference 18). The example data are shown below in Appendix C, Figure 2.

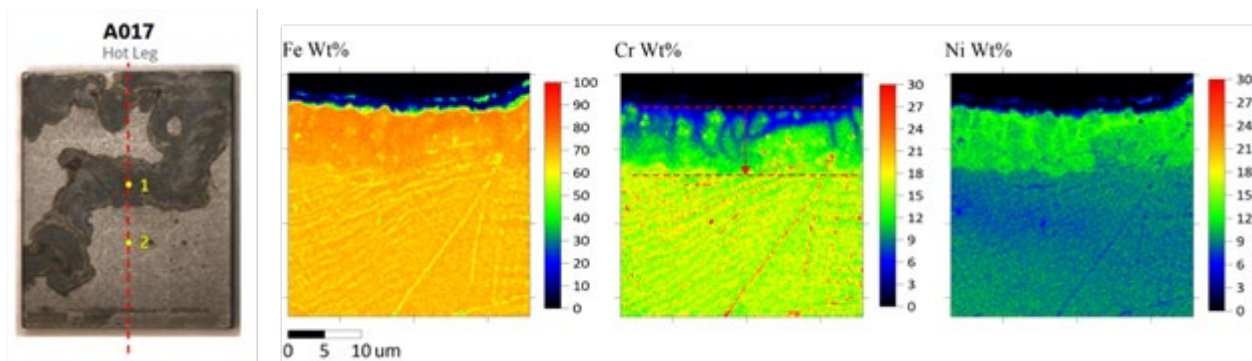
An example of how these data may be fit is via Appendix C, Equation C-1. In Equation C-1, A is a fitting constant, t is the exposure time, n is a fitting constant (equal to 0.5 for mass diffusion control), Q is the apparent activation energy, R is the gas constant and T the temperature.

$$Cr\ loss\ depth = A * t^n * EXP(-Q/RT) \quad Eq.\ C-1$$

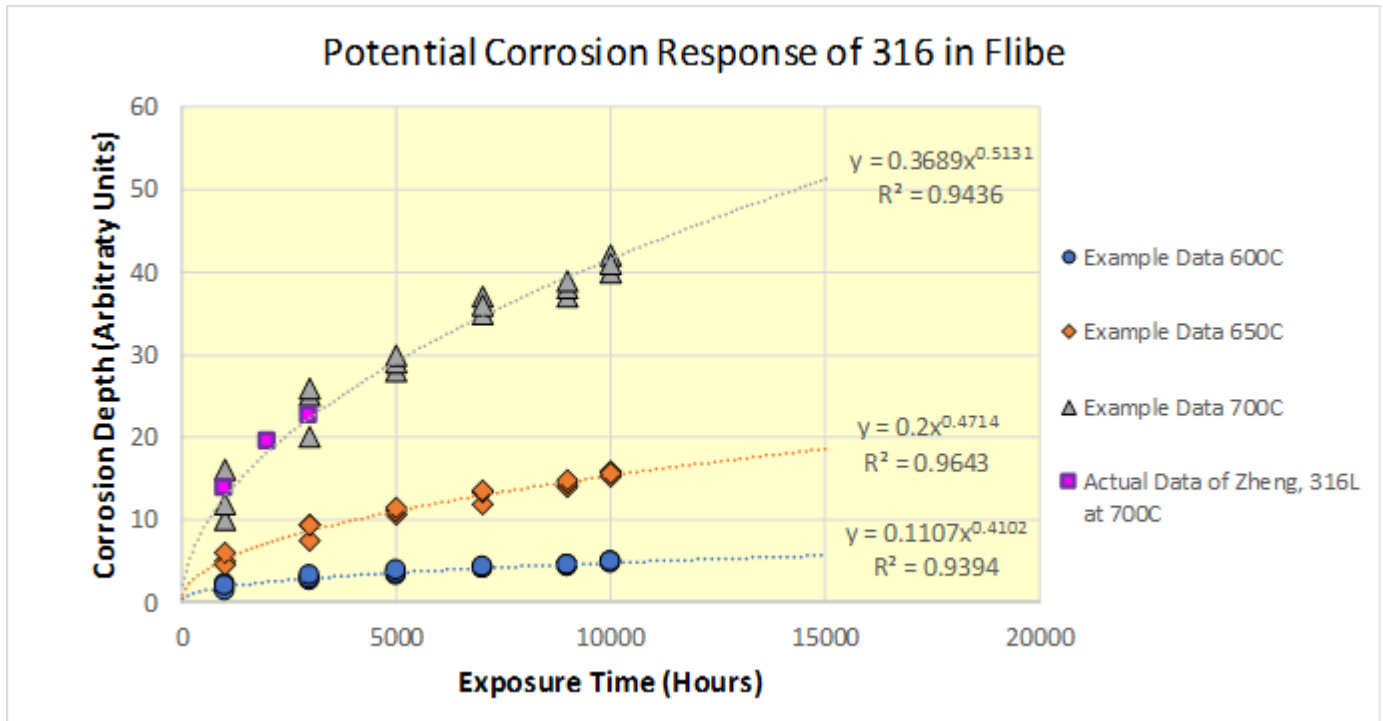
The fit of the data to the combined model is shown by the blue surface in Appendix C, Figure 3. In this manner all the data (example data in gray circles, Zheng data in pink squares) can be used to increase the confidence in extrapolating to the conditions of the KP-FHR. For example, the reactor vessel will operate

at approximately 550°C for [[]]] which would exhibit <10 microns of corrosion (Cr loss) via the best estimate prediction of this model. The example baseline model is shown in two dimensions in Appendix C, Figure 4 (upper graph) with 95% prediction intervals. In Appendix C, Figure 4, an example of a separate effects corrosion test is shown (lower plot) along with how a factor of improvement may be defined. In this example, the factor of improvement is conservatively determined at an exposure time within the data and between the baseline model lower bound and the separate effects test upper bound.

Appendix C Figure 1. Example of How a Corrosion Coupon was Sectioned (left) and Corresponding Compositional Maps for Iron, Chromium, and Nickel

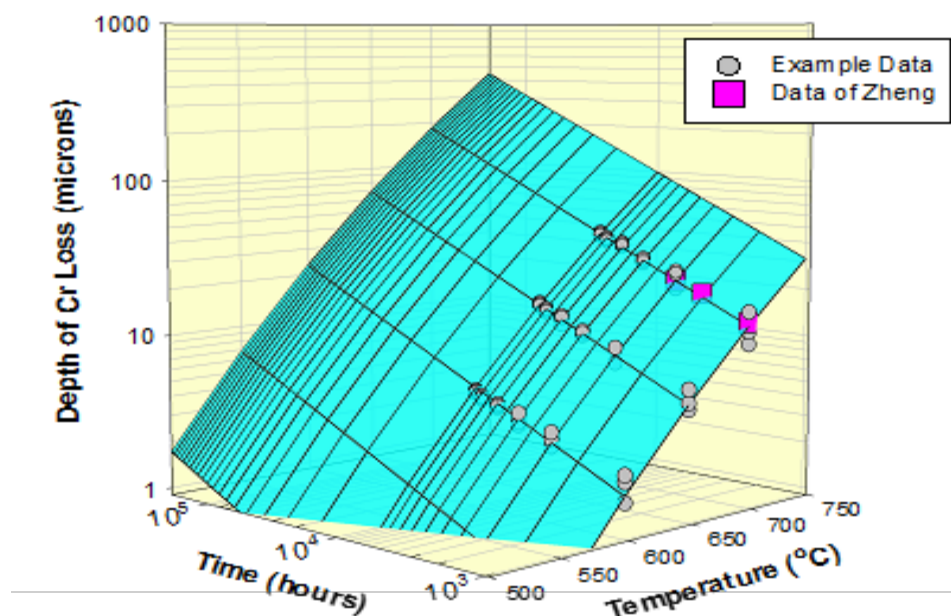


Appendix C Figure 2. The Corrosion Data of Alloy 316L in Flibe of Zheng (Pink Squares) Compared to Example Data at Three Different Temperatures

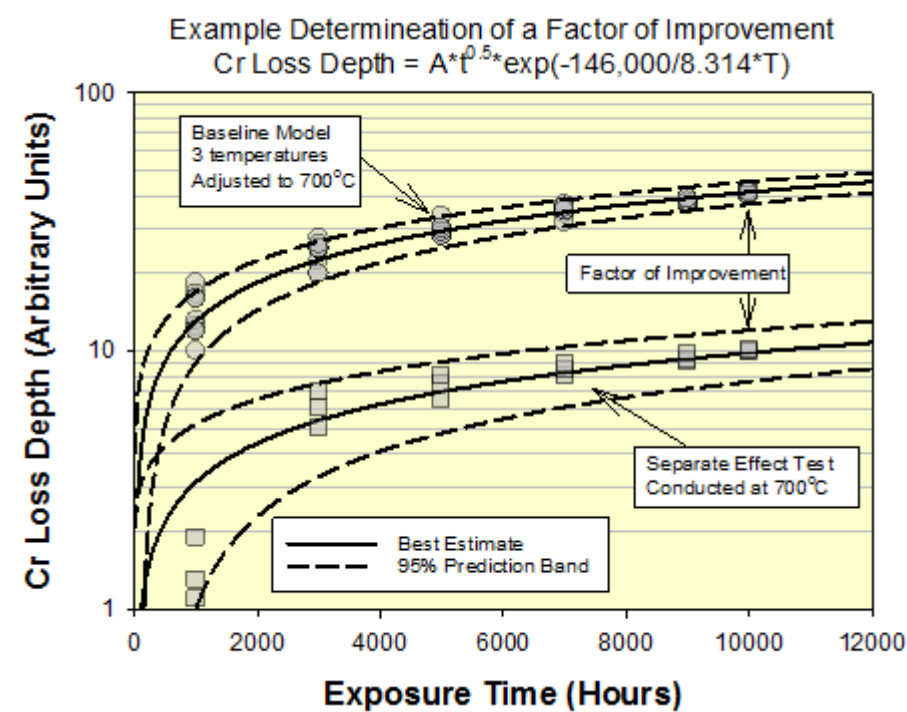


Appendix C Figure 3. Example of How Corrosion Data May be Fit and Extrapolated to Times Out to 20 years

**Example Fitting and Extrapolation of Corrosion Data
for Development of 'Baseline' Corrosion Response**



Appendix C Figure 4. Example of How the Baseline Corrosion Model May be Compared to a Separate Effects Test to Determine a Factor of Improvement



APPENDIX D. DELETED

APPENDIX E. TESTING AND ANALYSIS REQUIREMENTS FOR THE NON-POWER TEST REACTOR

This details how the qualification plan for structural alloy changes to support a non-power test reactor. The non-power test reactor is a lower power, shorter component life cycle system, which uses the same basic design and materials as the power generation reactor. Key points regarding the non-power reactor design are as follows:

- 7 – up to 35 MW_{th} design (versus 320MW_{th} for the commercial power reactor).
- Materials of construction are the same, i.e., TRISO fuel, graphite reflector, Flibe as the primary coolant, and Alloy 316H / ER16-8-2 stainless-steel vessel.
- Approximate 10-year lifetime (versus [[]] for the commercial power).
- The hot-leg outlet temperature of the Flibe 600-650°C, the cold leg temperature is ≤ 550°C. The average hot leg temperature is expected to be significantly < 650°C, i.e. significantly lower on average than the power reactor.

Based on these design changes, the following assumptions are made regarding operating conditions that could affect the performance of the structural alloys in safety-related components:

- Degradation due to irradiation will be significantly less than the power reactor.
- The stresses will be ≤ the power reactor.
- The average hot let temperature will be < the power reactor.
- The time at temperature will 2x-4x less than the power reactor.
- The Flibe flow rate will be ≤ the power reactor.
- The operating tempo of non-power test reactor is similar-to or more benign than the power reactor (e.g., the number of large thermal transients is low; therefore no new low cycle or high cycle fatigue concerns)
- The non-power test reactor heat rejection system does not adversely affect the composition of the primary coolant or the function of the safety related components (e.g., there is no increased risk for a large leak path into the Flibe salt).
- The non-power test reactor design and operation includes utilizing surveillance coupons to help ensure materials performance (metal and graphite samples exposed).
- The non-power test reactor design has a Reliability and Integrity Management Program that included enabling features like ‘design for inspection’ (e.g., locations to assess key attributes via NDT such as vessel wall thickness and weld integrity).
- The non-power test reactor vessel does not exhibit penetrations or deleterious design features (notches) below the salt level that could be prone to stress relaxation cracking.

With these assumptions, significantly less work is required to qualify the structural alloys used in safety-related components relative to the higher power, longer lived power reactor design (Appendix E, Table 1). For the non-power test reactor qualification program, two changes relative to the power reactor plan will be made:

[[

]]

[[

]]

Corrosion Testing

[[

]]

[[
]]

[[

]]

Environmentally Assisted Cracking Testing

Since environmentally assisted cracking of structural alloys in Flibe is relatively unexplored, there are no expected changes to the testing plan. However, tests under aggressive conditions (e.g., 600°C tests and slow stroke rates for the SSRT tests) will be prioritized over less aggressive conditions. The test matrices for the slow strain rate test and fracture mechanics-based corrosion fatigue / stress corrosion tests are reproduced in, Appendix E Table 3 and Table 4.

For the non-power reactor, the creep tests in nominal Flibe for the power reactor will be eliminated (Appendix E, Table 5). This change is due primarily to the shorter lifetime of the non-power test reactor and the fact that structural alloys will be exposed to redox controlled Flibe for the majority of their lifetime. Despite eliminating these tests, any potential interaction between creep-rupture and exposure to Flibe is expected to be captured in the planned slow strain rate testing. In those tests, any potential acceleration of the creep rate will be captured by the comparison of the deformation (e.g., the load vs. stroke) curves between samples exposed in air and samples exposed to Flibe.

Metallurgical Effects (previously 'Other')

In the power reactor testing plan, potential metallurgical degradation mechanisms were identified including stress relaxation cracking as well as pickup of beryllium and/or carbon by the stainless steel. The test matrix initially proposed to assess the risk of stress relaxation cracking, as well as the expected benefit of a post-weld heat treatment (Appendix E, Table 6). This testing will be eliminated for the non-power test reactor design. Instead, based on further literature review, the risk will be assessed based on weld joint design, welding process control and if required, finite element analysis. Mitigation of stress relaxation cracking concern via design and analysis is well accepted in the literature. For example, an index like the 'Spindler Fraction' has been shown to correlate with the occurrence of stress relaxation

cracking (Reference 49 and 52) and if triaxial stresses can be minimized, the risk of cracking is eliminated. This strategy is presented in more detail below.

For the non-power reactor, the welds of interest for stress relaxation cracking may be a longitudinal seam weld in the pressure vessel (if that method of construction is chosen) or a circumferential weld between the lower head and the vessel. These are the only potential welds of interest since welds on the upper head do not present a risk of draining the salt from around the fuel pebbles. As shown in Figure 23 the lower head to vessel weld from the internal radius of the bottom head will be separated such that there is no stress concentration in the weld heat affected zone. Without a stress concentrating feature for this weld (or an extensive weld repair when constrained) there is no mechanism by which significant triaxial stresses can develop in the thru wall direction of a thin-walled pressure vessel. Note that the concern of weld repair generating triaxial stresses will be mitigated via welding process control and, if required, finite element analysis of the repair. Without a triaxial stress state, the risk of stress relaxation cracking in Alloy 316H stainless steel heat affected zones is effectively mitigated (Reference 41). Furthermore, the potential weld residual stresses for the non-power reactor will be further evaluated via finite element analysis.

To further emphasize the difference between the expected stresses on the non-power reactor vessel and industrial observations of stress relaxation cracking in Alloy 316H, Appendix E, Table 10 compares the expected non-power reactor stresses with known stresses that have resulted in stress relaxation cracking. In Appendix E, Table 10 two metrics are used to assess the risk of stress relaxation cracking: (1) the ‘Spindler Fraction’ (S) where there is risk for cracking when $S < 0.3$ (Reference 62 and 63) and (2) the ratio of the elastic follow-up factor (Z) to the Spindler fraction where there is risk when $Z/S > 10$ (Reference 64). As shown, both metrics indicate no risk of stress relaxation in the non-power reactor vessel but clear risk for the industrial observations of cracking in Alloy 316H.

[[

]]

Irradiation Effects

While the power reactor plan proposed testing for irradiation induced embrittlement, the shorter lifetime and lesser irradiation damage of the non-power test reactor enables these concerns to be addressed through existing literature data and validated via surveillance sample testing. The testing that is proposed to be eliminated is provided in Appendix E, Table 8, and Table 9. Note that the timing of the surveillance sample program is currently being developed but initial test data on potential effects on corrosion and stress corrosion cracking are expected to be available within 5 years of reactor startup.

The planned surveillance sample testing for non-power test reactor will also inform the design and licensing of the power reactor power reactor. For the power reactor application, the longer operating life [[]] as well as the higher power operation make the irradiated material performance data desirable. These surveillance sample data from the non-power test reactor are expected to retire the risk of irradiation affected corrosion, irradiation assisted stress corrosion cracking, and to enable more accurate determination of the expected degradation in creep life due to helium embrittlement. The non-power test reactor surveillance samples are currently the only opportunity to assess the combined effects

of exposures to Flibe and irradiation. However, it should be noted that Kairos Power is currently in discussions with the Idaho National Laboratory to utilize a planned April 2022 irradiation campaign in the Advanced Test Reactor. That work could help assess the irradiation performance of both Alloy 316H and ER16-8-2 via both irradiated materials testing and ex-situ irradiation + Flibe exposure for concerns like irradiation affected stress corrosion cracking.

Conclusions for the Non-Power Test Reactor

This Appendix details the proposed changes in the testing required to qualify Alloy 316H / ER16-8-2 for use in the non-power reactor, a shorter-lived test reactor design, as compared to the commercial power reactor. Due to the shorter lifetime and lesser irradiation damage of the non-power reactor, several tests have been reduced in scope or eliminated. In summary, the proposed changes are as follow:

[[

]]

Appendix E Table 1. Areas to Address Based on the KP-FHR Metallic Materials Qualification Plan

[[

]]

Appendix E Table 2. Changes to the Corrosion Testing Plan for the Non-Power Test Reactor

[[

]]

Appendix E Table 3. Summary of Planned Slow Strain Rate Tests to Assess the Potential for Environmentally Assisted Cracking on both the Non-Power Test Reactor and Power Reactor

[[

]]

Appendix E Table 4. Summary of Planned Corrosion Fatigue and Stress Corrosion Cracking Tests to Assess the Potential for Environmentally Assisted Cracking in the Non-Power Test Reactor and Power Reactor

[[

]]

Appendix E Table 5. The Environmental Creep Tests that are Eliminated for the Non-Power Test Reactor

[[

]]

Appendix E Table 6. Testing to Assess Stress Relaxation Cracking that are Delayed or Eliminated for the Non-Power Test Reactor

[[

]]

Appendix E Table 7. Summary of the Proposed Changes to Metallurgical Effects Tests for the Non-Power Test Reactor

[[

]]

Appendix E Table 8. Proposed Elimination of the Irradiation Embrittlement Testing Plan for the Non-Power Test Reactor

[[

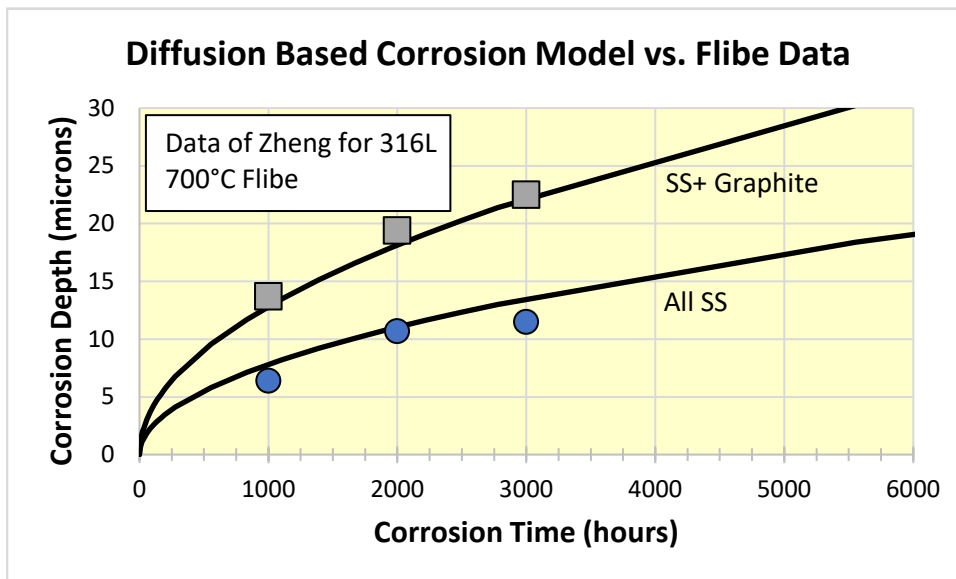
]]

Appendix E Table 9. Proposed Elimination of the Irradiated Creep Tests for the Non-Power Test Reactor

[[

]]

Appendix E Figure 1. Good Fit Between a Grain Boundary Diffusion-Based Corrosion Model for Chromium Loss (solid lines) and the Corrosion Data for Alloy 316L in Flibe



Note: From Zheng et al.

Fitted lines:

$$Q = 260 \text{ kJ/mol}$$

$$D_0 = 10.2 \text{ cm}^2/\text{sec}$$

$$C_0 = 17 \text{ wt.\% Cr}$$

$$C(x,t) = 15 \text{ wt.\% Cr}$$

$$C_s \text{ SS} = 12 \text{ wt.\% Cr}$$

$$C_s \text{ graphite} = 5 \text{ wt.\% Cr}$$

APPENDIX F. CERTIFIED MATERIAL REPORTS

Appendix F Figure 1. Material Certification Report for Alloy 316H Plate

[[

]]

Appendix F Figure 2. Overcheck of the Composition of the Alloy 316H Plate

[[

]]

]]

Appendix F Figure 3. Material Certification Report for the ER16-8-2 Weld Wire

[[

]]

Appendix F Figure 4. Material Certification Report for Second Heat of ER16-8-2

[[

]]

Appendix F Figure 5. Material Certification Report (tentative) for a Third Heat of ER16-8-2

[[

]]